International Journal of
Molecular Sciences

MDPI

Review

Ion and Water Transport in Ion-Exchange Membranes for Power Generation Systems: Guidelines for Modeling

Semyon Mareev [1,2], Andrey Gorobchenko [1,2], Dimitri Ivanov [2,3,4], Denis Anokhin [2,4,5] and Victor Nikonenko [1,2,*]

1 Membrane Institute, Kuban State University, 350040 Krasnodar, Russia
2 Faculty of Fundamental Physical and Chemical Engineering, Lomonosov Moscow State University, 119991 Moscow, Russia
3 Institut de Sciences des Matériaux de Mulhouse-IS2M, CNRS UMR 7361, Jean Starcky, 15, F-68057 Mulhouse, France
4 Center for Genetics and Life Science, Sirius University of Science and Technology, 1 Olympic Ave, 354340 Sochi, Russia
5 Institute of Chemical Physics Problems of RAS, Acad. Semenov Av., 1, 142432 Chernogolovka, Russia
* Correspondence: v_nikonenko@mail.ru; Tel.: +7-918-41-45-816

Abstract: Artificial ion-exchange and other charged membranes, such as biomembranes, are self-organizing nanomaterials built from macromolecules. The interactions of fragments of macromolecules results in phase separation and the formation of ion-conducting channels. The properties conditioned by the structure of charged membranes determine their application in separation processes (water treatment, electrolyte concentration, food industry and others), energy (reverse electrodialysis, fuel cells and others), and chlore-alkali production and others. The purpose of this review is to provide guidelines for modeling the transport of ions and water in charged membranes, as well as to describe the latest advances in this field with a focus on power generation systems. We briefly describe the main structural elements of charged membranes which determine their ion and water transport characteristics. The main governing equations and the most commonly used theories and assumptions are presented and analyzed. The known models are classified and then described based on the information about the equations and the assumptions they are based on. Most attention is paid to the models which have the greatest impact and are most frequently used in the literature. Among them, we focus on recent models developed for proton-exchange membranes used in fuel cells and for membranes applied in reverse electrodialysis.

Keywords: charged ion-exchange membranes; mathematical modeling; energy production and storage; ion and water transport; structure-property models; transport equations; conductivity; permeability; permselectivity

check for updates

Citation: Mareev, S.; Gorobchenko, A.; Ivanov, D.; Anokhin, D.; Nikonenko, V. Ion and Water Transport in Ion-Exchange Membranes for Power Generation Systems: Guidelines for Modeling. *Int. J. Mol. Sci.* **2023**, *24*, 34. https://doi.org/10.3390/ijms24010034

Academic Editor: Andreas Taubert

Received: 15 November 2022
Revised: 12 December 2022
Accepted: 17 December 2022
Published: 20 December 2022

Copyright: © 2022 by the authors. Licensee MDPI, Basel, Switzerland. This article is an open access article distributed under the terms and conditions of the Creative Commons Attribution (CC BY) license (https://creativecommons.org/licenses/by/4.0/).

1. Introduction

Ion exchange membranes (IEMs) are widely used in water treatment and energy storage/generation systems. Water treatment, desalination and concentration of solutions, ion separation and some other applications are carried out using electrodialysis (ED) [1–4]. As for energy storage and generation, proton-exchange membrane (PEM) electrolysis, reverse electrodialysis (RED), redox flow batteries (RFB), fuel cells (FC) and some other membrane processes are applied [5–13] (Figure 1). In ED (Figure 1a), the feed solution components are transferred through alternating cation-exchange (CEM) and anion-exchange membranes (AEM) under the action of an external electric field [1–4]. As a result of this process, the feed solution is concentrated in some compartments (concentration compartments) and desalinated in others (desalination compartments). Therefore, ED is also considered as a process associated with energy storage. Such features of ED make it an attractive technology for application in various fields [7]: water desalination (sea water, well water,

brackish water, etc.); wastewater treatment (industrial, agricultural, municipal wastes); food industry (wine, dairy, production of juice drinks, etc.); medicine (purification of amino acids, desalination of pharmaceutical intermediates, recovery of blood plasma proteins, etc.); electronic industry (purification of water for electronics processing); production of ultrapure water and many other areas. In RED (Figure 1b) no external electric field is applied, and alternating CEM and AEM separate the concentrated feed (e.g., sea water) and the dilute feed (e.g., river water) solutions. Species diffusion through a membrane causes ionic fluxes from a concentrated solution to a dilute one, and the energy released during this process generates electricity [14]. Both the counter-current operation of the RED (when sea and river water in the corresponding compartments flow in opposite directions as presented in Figure 1b) and co-current mode (co-directional flow of sea and river water in the respective compartments) are used. However, as shown in Ref. [15], the co-current mode is preferable as it allows greater productivity. Power generation is an application of RED, but there are some specific applications [16]: RED designed to produce hydrogen and store energy in batteries; RED for wastewater treatment using electricity in situ; and various combinations of RED with other desalination technologies. By analogy with ED, PEM electrolysis (Figure 1c) is associated with energy storage [10], and FC (Figure 1d) with its production [17,18]. In PEM electrolysis, water molecules are fed into the anode catalyst layer, where they are oxidized to oxygen and protons, i.e., an oxygen evolution reaction (OER) takes place:

$$H_2O \rightarrow 2H^+ + 1/2O_2 + 2e^-. \quad (1)$$

The resulting oxygen is removed from the device, and the protons are transferred by an electric field through the PEM to the cathode catalyst layer, where they are reduced to hydrogen, i.e., a hydrogen evolution reaction (HER) takes place:

$$2H^+ + 2e^- \rightarrow H_2. \quad (2)$$

In FC with PEM, the opposite occurs: hydrogen is fed into the anode catalyst layer, where it is oxidized to protons, a hydrogen oxidation reaction (HOR):

$$H_2 \rightarrow 2H^+ + 2e^-. \quad (3)$$

As a result of this reaction, heat and a direct electric current are generated. The resulting protons are transferred through the PEM to the cathode catalyst layer, where oxygen is also supplied. As a result, an oxygen reduction reaction (ORR) takes place in the cathode layer with the formation of water:

$$2H^+ + 2e^- + 1/2O_2 \rightarrow H_2O. \quad (4)$$

As for RFB, their application is related to both generation and storage of energy. Aqueous RFB (Figure 1e) is a sandwiched structure consisting of positive and negative porous carbon electrodes separated by an ion-exchange membrane. The external reservoirs contain electrolytes with dissolved active species that circulate through the porous electrodes. Electrochemical reactions take place on the electrodes to store or release electricity. The energy storage tanks are separated from the power pack; therefore, the stored energy can be scaled [17].

The use of IEMs in these applications is due to their ability to enhance or impede species transfer not only because of the size of the species, but also because of their charge.

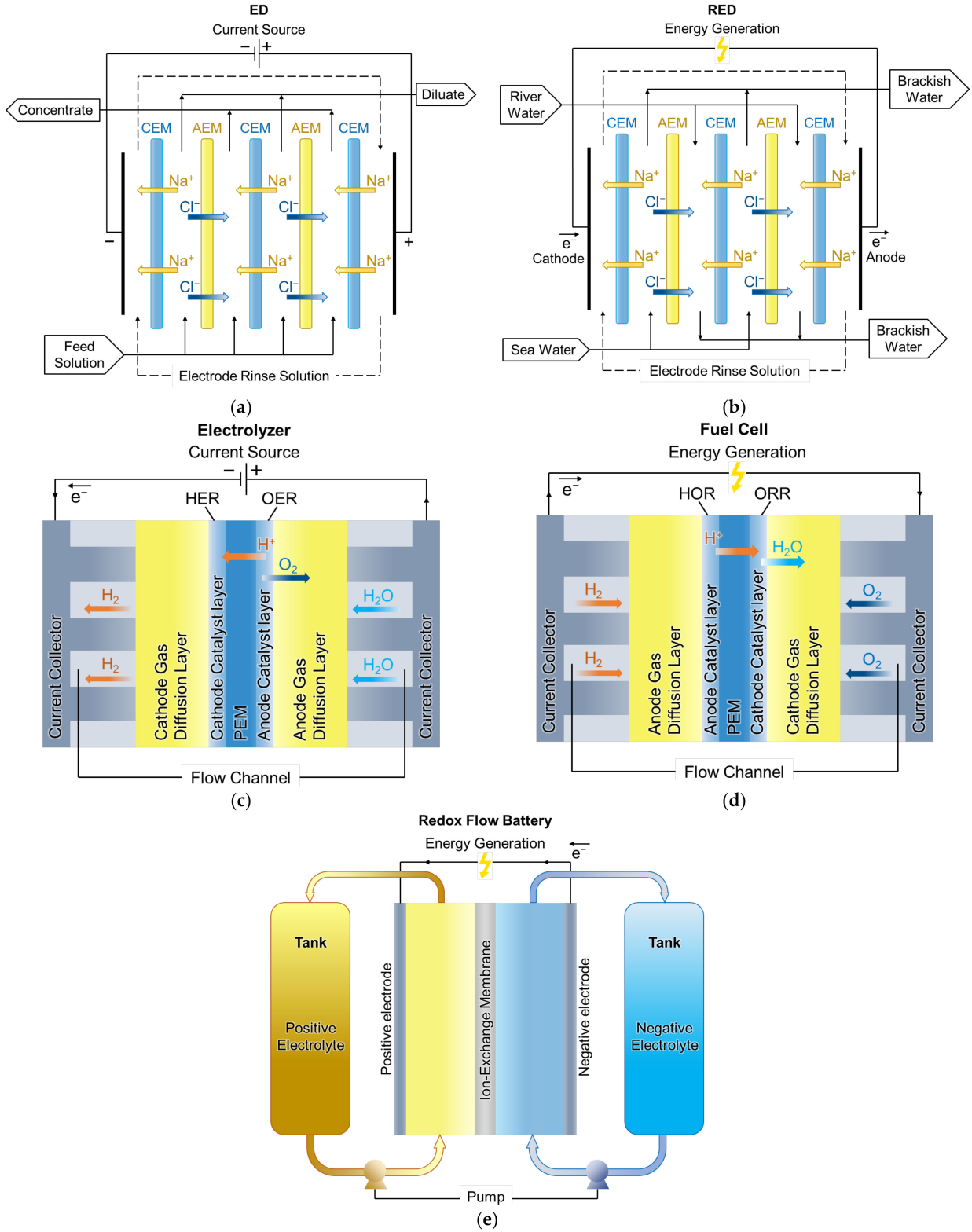

Figure 1. Scheme and principle of operation of the main membrane devices related to energy production and storage: conventional electrodialysis (**a**), reverse electrodialysis (**b**), PEM electrolyzer (**c**), fuel cell (**d**), and redox flow battery (**e**).

Synthetic ion exchange membranes (IEMs) are polymeric materials whose structure is based on aliphatic, aromatic or perfluorinated residues containing functional groups ($–SO_3^-$, $–NH_3^+$ and others). These functional groups are fixed due to strong chemical

bonds with the polymer matrix, and the presence of a charge in such a group allows it to participate in exchange reactions with ions from an external solution (Figure 2).

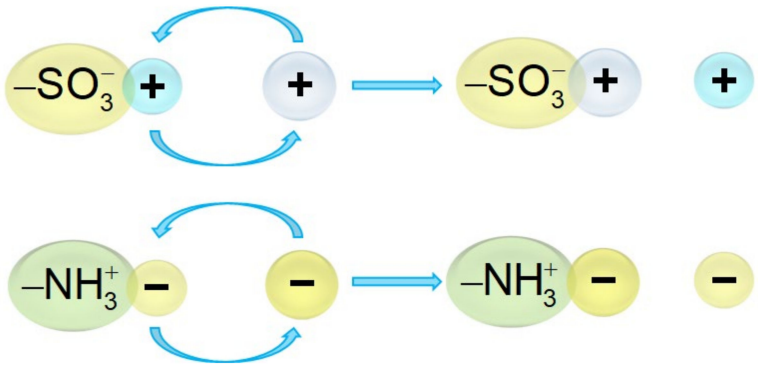

Figure 2. Schematic representation of exchange reactions on fixed membrane groups.

Depending on the sign of the charge of the functional groups fixed to their matrix, membranes are divided into cation-exchange (negative fixed charge) and anion-exchange (positive fixed charge). A detailed description of the structure and types of polymer chain architecture of various cation and anion exchange membranes was provided in the review by Ran et al. [19]. The authors distinguish the following types of polymer chain architectures for CEMs: block CEMs, side chain type CEMs, comb-shaped CEMs and densely functionalized CEMs. The types for AEMs include side chain type AEMs, comb-shaped AEMs, AEMs with dense grafting of anion conducting groups, multi-block AEMs, AEMs with long aliphatic chains, and AEMs with dual-cation containing side chains. The authors [19] showed that differences in the topological architecture of polymer ionomers significantly affect the overall performance of CEMs and AEMs.

According to the structural features and method of production, membranes are traditionally divided into homogeneous and heterogeneous. Homogeneous membranes are usually produced by copolymerization of monomers. There are two types of such IEMs: single-phase (Nafion, DuPont Co., Wilmington, California, USA; MF-4SK, Plastpolimer, St. Petersburg, Russia, and others) consist of a continuous layer of ion exchange material (homogeneous at the micrometer scale) with more or less evenly distributed fixed groups; and two-phase (Neosepta AMX, CMX, Astom, Tokyo, Japan; CJMCED, CJMAED, Hefei ChemJoy Polymer Materials, Hefei, China; and others), with a structure that, along with a sulfonated polymer, may include an inert binder and reinforcing fibers [20,21]. Heterogeneous membranes are produced by mixing microgranules (about 5–50 μm) of an ion exchange resin with an inert binder (MK-40, MA-40, Shchekinoazot, Russia; Ralex CMH, AMH, MEGA a.s., Czech Republic, and others) [21]. These IEMs may be reinforced with meshes or fabrics made of various polymers (polyester, capron, lavsan, polyvinyl chloride, and others) to achieve high mechanical strength. Such a structure leads to significant differences in physicochemical properties of membrane bulk and surface on a micrometer scale. There are both electrically conductive and non-conductive areas corresponding to the phase of the ion exchanger and the inert binder, respectively, and the presence of a reinforcing fabric contributes to the development of geometric heterogeneity (waviness) of the surface. This kind of heterogeneity may contribute to the development of electroconvection in electromembrane systems [22,23].

It should be noted that despite the presence of two phases in the structure of the material, Neosepta, CJMCED, CJMAED and other similar membranes are still traditionally called homogeneous [3,7]. However, “homogeneous” membranes, strictly speaking, are inhomogeneous on the 10–100 nm scale. When swollen in an aqueous solution, they contain hydrophilic pores/channels enclosed in a hydrophobic matrix. These pores/channels allow the transport of ions and water across the membrane [24].

The characteristics of the IEM are determined by the requirements of the process in which they are applied [9]. There are membranes of several special grades, which are used in different applications. In electrodialysis water desalination, a membrane stack with alternating cation-exchange and anion-exchange membranes (CEM and AEM) is used. Cations pass through the cation-exchange membrane, and anions through the anion-exchange membrane. Thus, ED requires membranes that provide counterion/coion selectivity [25]. At the same time, there are many applications where the permselectivity for a specific ion is needed. For example, the separation of monovalent and multivalent ions of the same sign of charge (such as Na^+ and Ca^{2+}) is required for water softening. This separation is achieved with the use of special-grade membranes, monovalent-ion-selective membranes, which are used in a process called selectrodialysis [26]. Achieving ideal membrane permselectivity is hindered by high water content. The higher the water content, the more the membrane swells. Swelling of the membrane leads to an increase in permeability, which is usually accompanied by a partial loss of selectivity. Thus, there is a trade-off between the permselectivity and permeability of membranes [27,28], which forces researchers to look for the optimal ratio of these characteristics.

In the electrodialysis production of alkalis and acids, other special-grade membranes, bipolar membranes, are used. Their purpose is the generation of H^+ and OH^- ions, and an important property is an increased catalytic activity for the water dissociation reaction [29]. Vanadium redox flow batteries [12] use IEMs that allow catholyte and anolyte solutions to exchange charge-balancing species (e.g., protons through CEMs and sulfate/bisulfate through AEMs), but not active redox vanadium ions. In proton-exchange membranes used in fuel cells and electrolysis, in addition to ions, it is important to control the transfer of water and/or neutral solutes [30,31]. Moreover, PEMs in fuel cells must maintain stable properties at high temperatures [32].

With such diverse requirements for IEMs, the challenge for researchers is to improve understanding of the fundamental properties of membranes responsible for various desirable or undesirable effects. The purpose of this review is to help researchers the use of mathematical modeling and simulation as effective tools to enhance this understanding. The paper discusses the relationships between membrane structure and their properties using basic equations and well-established models for their classification. With that, new approaches to the description of transport phenomena in charged membranes are reviewed. The main attention is focused on the models related to energy generation applications. Related phenomena such as chemical reactions (water splitting, acid dissociation, etc.) are also considered.

2. Structure of IEMs

IEMs are self-assembling nanostructured materials composed of macromolecules [33]. The structure, and hence the properties, of biological membranes and IEMs have some similarities [34]. The main components of the structure of biological membranes are amphiphilic compounds that have both hydrophilic and hydrophobic components (Figure 3). They consist of a phosphate 'head' (circles in Figure 3b) and a lipid 'tail' (lines) that are, compatible and incompatible with water, respectively.

The main structural element of the functional part of IEMs is a hydrophobic base, consisting of hydrocarbon (such as in Neosepta membranes, Astom) or perfluorinated (such as in a Nafion®, Dupont) chains. The charged functional groups make up the hydrophilic part of the IEM. Due to the flexibility of polymer chains, this combination ensures self-organization in the membrane bulk [35]. The polymer chains form the matrix of the membrane, while the functional groups are assembled into clusters, the size of which is on the order of several nanometers. In an aqueous solution, the hydrophilic functional groups become hydrated and the membrane swells. The size of the clusters increases, conducting channels appear between them, and they form a percolation system when a certain water content is reached [36]. Therefore, the hydrophobic components contribute to the morphological stability of the membrane, and hydrophilic components create a

system of conducting channels. The degree of swelling depends on the concentration of the external solution: with an increase in the concentration of the solution, the water content in the IEM decreases [37]. If the membrane contains weakly basic functional groups, such as secondary and tertiary amino groups, there is a dependence of the water content on the pH of the external solution [38,39].

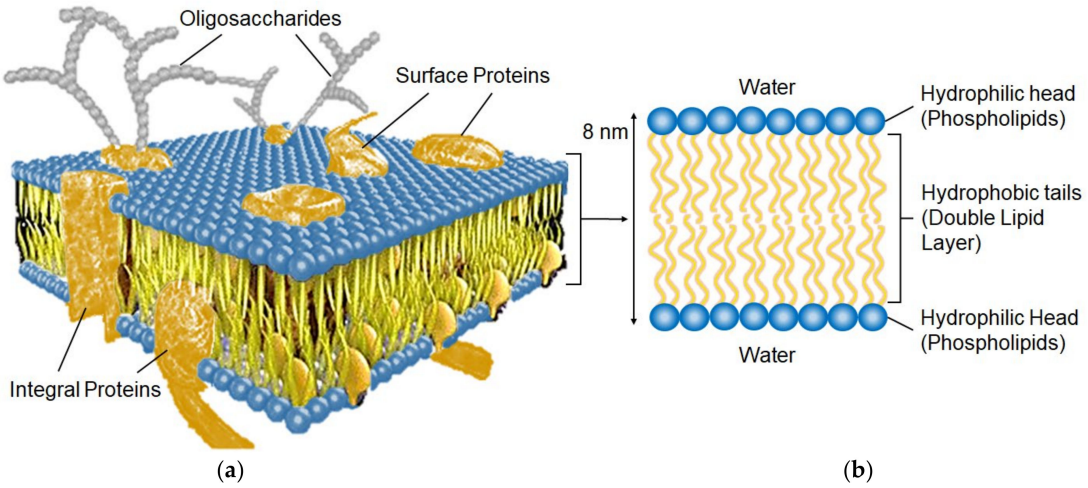

Figure 3. Schematic representation of a biological membrane (**a**) and lipid bilayer (**b**).

The cluster and channel model, first proposed by Gierke in [40], describes the main features of the behavior and adequately explains the transport properties of Nafion® membranes [24]. The main idea of the existence of relatively large agglomerates/clusters of functional groups (several nanometers or more), which are connected by narrower channels (about 1 nm in diameter) (Figure 4), can be also applied to most other IEMs. Kreuer developed a more detailed representation of the two-dimensional structure of Nafion® [41], which generally corresponds to the Gierke model [40]. Clusters, channels, some structural defects, gaps between ion-exchange resin particles, binder and tissue form a system of pores in IEM, the size of which varies from a few nm to 1–2 microns [42–44].

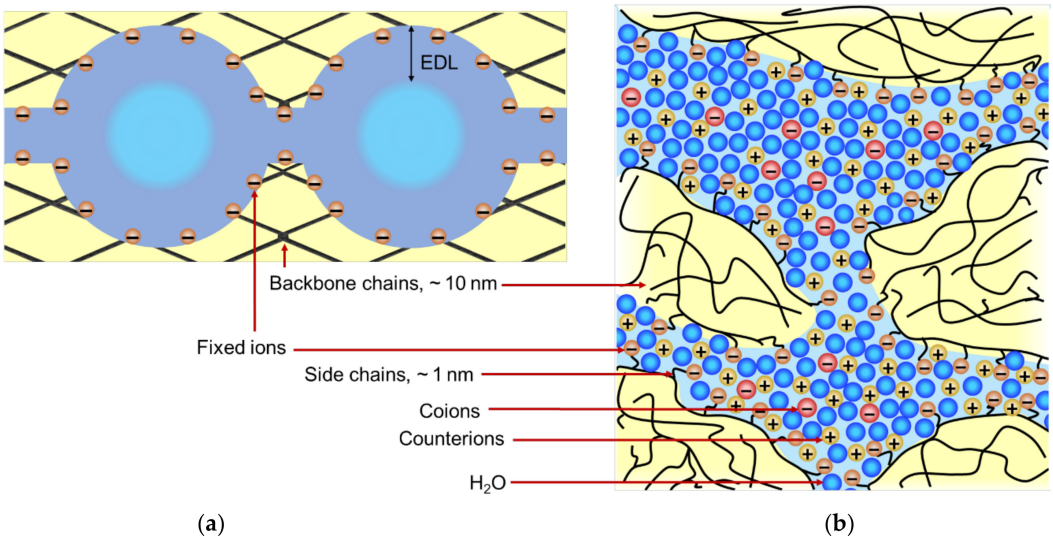

Figure 4. Schematic representations of Nafion® structure proposed by Gierke (**a**) [45] and Kreuer (**b**) [41]. An electrical double layer (EDL) is formed at the charged pore wall, and an electrically neutral solution is present in the center of the pore.

There is an analogy of the structure of polymer side chains with a fixed functional group (Figure 5a) and phospholipid molecules of biomembranes (Figure 3b): both contain a hydrophilic 'head' and a hydrophobic 'tail'.

Figure 5b shows that structuration of a membrane of the kind represented by Nafion® begins even in the dry state: functional $-SO_3H$ groups attract each other and form clusters because they are dipoles. The flexibility of polymer chains allows this to occur. With an increase in the membrane water content, hydrated clusters first form, then intercluster channels appear, and percolation occurs (Figure 5c). If the backbone polymer chains are not intertwined enough, with sufficient water content, the polymer can split into individual chains and dissolve.

The solution that fills the clusters, where fixed functional groups are concentrated, mainly contains counterions formed as a result of the dissociation of functional groups. The counterions in thermal motion are attracted to fixed charged groups, thus forming an electrical double layer (EDL) separating the fixed ions and electrically neutral solution. The latter can be present in the center of the cluster if the EDL thickness is smaller than the cluster radius (Figure 4a). The central part of the pore contains a small number of coions carrying a charge of the same sign as the fixed ions. Coions are repelled from the pore walls by electrostatic forces; this effect is called Donnan exclusion [37] and was first described in his paper in 1911 [46]. The distribution of ions inside the EDL is described by the Gouy–Chapman theory, which takes into account both electrostatic and thermal interactions. Figure 6a schematically shows the distribution of ions near the pore wall, represented as a charged plane. The concentration of counterions in the pore solution increases, and the concentration of coions decreases with a decrease in the ratio of the pore radius to the Debye length (Figure 6a). The latter characterizes the EDL thickness. Therefore, the smaller the pore radius, the higher the selectivity of the membrane (and the higher the resistance of the membrane). If the pore radius is greater than the Debye length, an electrically neutral solution is located in the center of the pore.

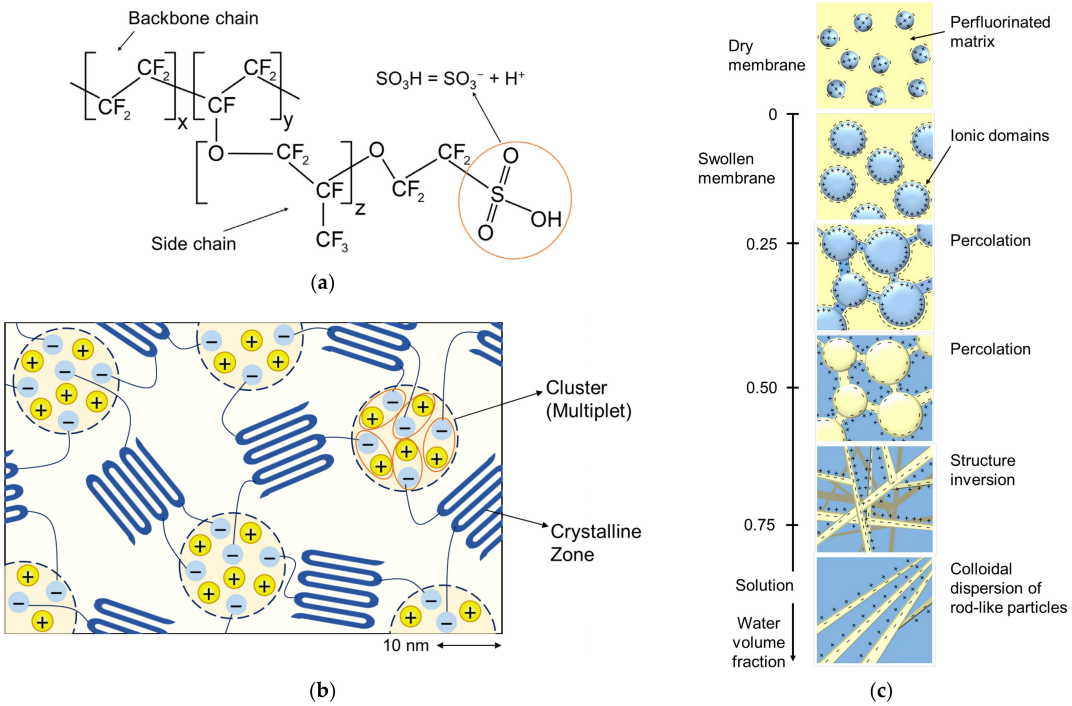

Figure 5. A perfluorinated sulfonated polymer (supra)molecule (**a**). Formation of nanoclusters in the dry state of a perfluorinated sulfonic-acid polymer (**b**) (redrawn from [47]). Evolution of the nanostructure of such a polymer during hydration (**c**) (redrawn from [36]).

Water molecules that are close to functional groups are structured and largely lose their mobility [24,34]. As a result, the relative permittivity ε decreases as the solution approaches the functional groups. The permittivity of the Nafion membrane was studied in detail by Paddison et al. [48]. It is shown that with increasing water content, ε increases linearly, starting from the value corresponding to the dry polymer (ε = 2.1 for polytetrafluorethylen (PTFE)) and increasing to the value that refers to the pore solution of the hydrated polymer (ε = 20 for Nafion®117) [49] (Figure 6b). The mobility of counterions concentrated near the functional groups is very low, mainly due to the strong electrostatic interaction [24]. The side chains also contribute to their low mobility, cluttering up the space [50]. Due to the finite size of hydrated counterions, their concentration decreases when the distance from the fixed group becomes less than about 0.5 nm. When approaching the center of the pores, the concentration of counterions also decreases in accordance with the Gouy–Chapman ion distribution law in the EDL (Figure 6a).

Water molecules located in the center of sufficiently large pores behave similarly to molecules in a free solution, and ε also approaches the value of 81, corresponding to an electrically neutral solution [51]. Grotthuss shuttling dominates the vehicular diffusion (solvation diffusion): the proton hops from one H_3O^+ (or $H_5O_2^+$ or even greater) complex to the neighboring one. Instead of moving in the aqueous environment, it transfers within the hydration shell [51].

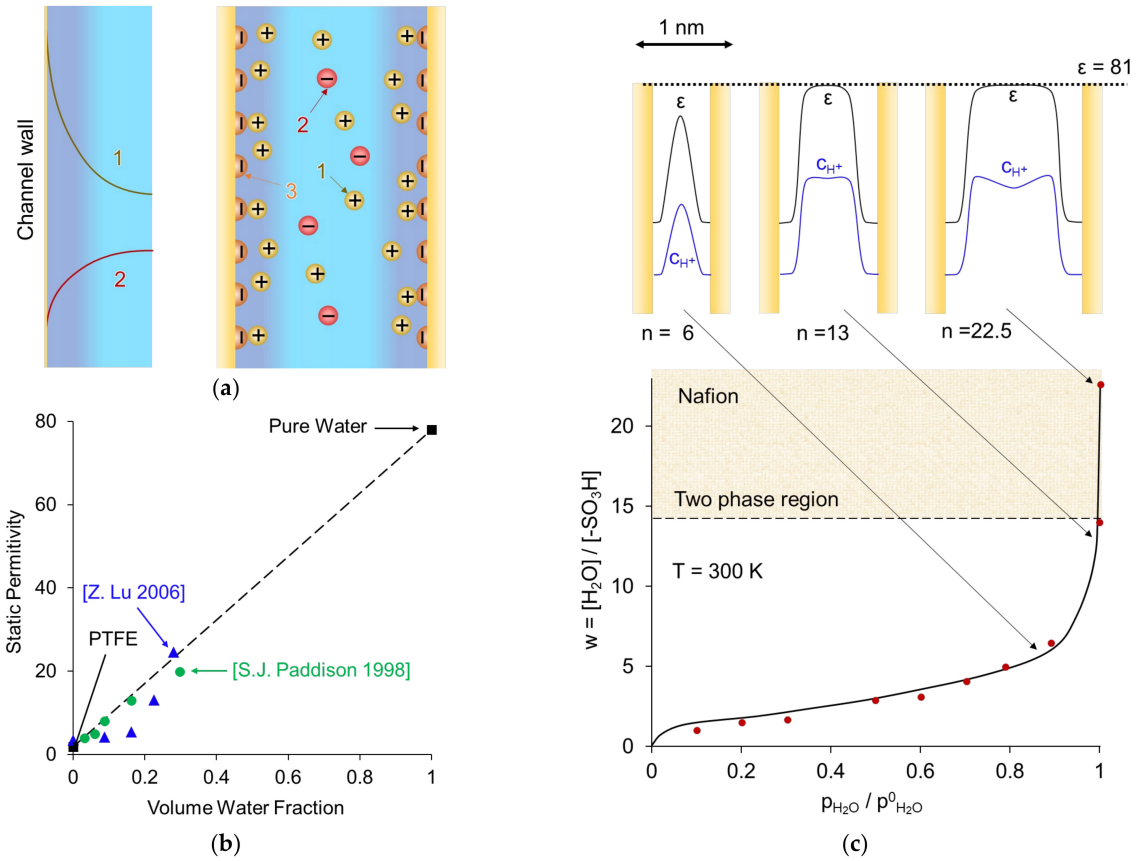

Figure 6. (**a**) Distribution of counterions (1) and coions (2) within a pore near a charged wall with fixed functional groups (3). Reproduced with permission from [52]. (**b**) Static permittivity of Nafion® 117 measured by by Padisson et al. [49] and Lu [53], plotted as a function of the volume fraction of water sorbed in the polymer. (**c**) Hydration isotherm (water content, *w*, as a function of relative water vapor pressure) for Nafion 117, and the distribution of the dielectric constant and proton concentration across the hydrated hydrophilic pores for three different values of n (top). A hydrated counterion is shown near the pore wall. Adapted from [24].

Electronic structure calculations [54] show that in perfluorinated membranes (such as Nafion®) 2–3 water molecules per sulfonic acid group (w) are needed for proton dissociation. The dissociated proton is separated from the sulfonate anion when six water molecules are added to the membrane. According to Kreuer et al. [24], only at $w > 14$ is there a two-phase system where free water is clearly distinguishable in the pore (Figure 6c).

A generalized representation of the structure of an IEM is shown in Figure 7. It is a fragment that includes hydrophobic domains of the matrix, micropores (where EDLs overlap) and mesopores (where EDLs do not overlap but occupy a significant part of the pore). This fragment is typical for homogeneous IEM, which usually do not contain macropores. Heterogeneous membranes, in addition to micro- and mesopores, also contain macropores, which can be spaces between the particles of the ion exchange resin and the reinforcing binder and fabric.

The counterion must overcome the potential barrier when moving from one functional group to another [55]. The value of this barrier depends on the energy of the electrostatic and chemical interactions between the hydrated counterion and the functional group and on the energy required to move polymer chains to form a sufficiently large ion transport channel or cluster in the membrane matrix. The average distance between two adjacent functional group depends on the exchange capacity and membrane morphology. For conventional membrane materials, this distance is in the range of 0.5–1.0 nm [34], in particular for the perfluorosulfonic membrane Nafion, it is about 0.8 nm [24,34].

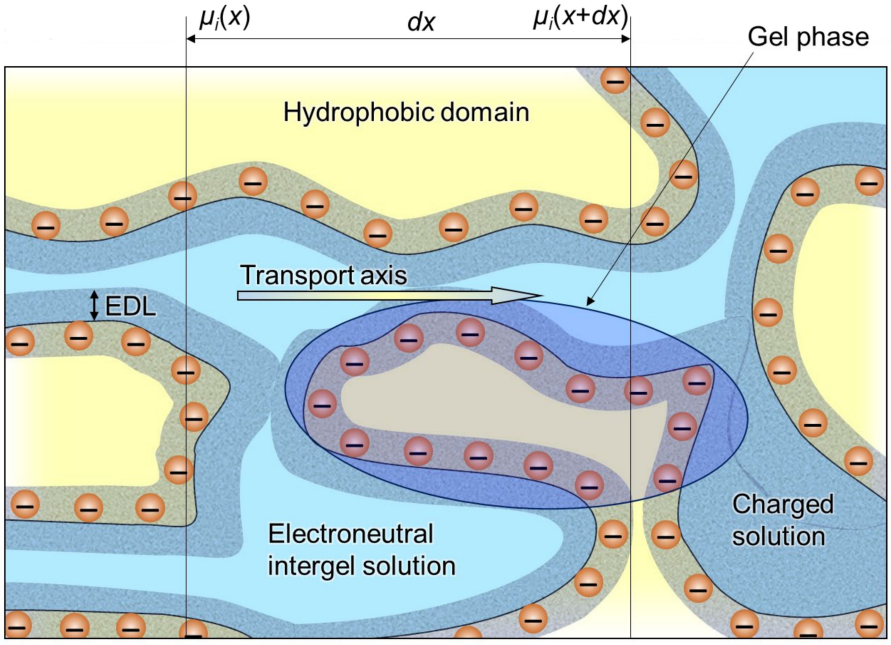

Figure 7. Schematic representation of the IEM structure with its main elements: fixed ions (shown as circles with "−"), EDL formed at the internal interfaces, and electroneutral solution in the center zone of intergel spaces. The gel phase includes the polymer matrix bearing the fixed ions and the EDL. Redrawn from [56].

The main characteristics of IEMs, such as permselectivity and conductivity, primarily depend on the ratio of the volumes of the central and near-wall parts of the liquid in the pores. A large fraction of the electroneutral central part, which is typical for big pores, reduces the permselectivity. With an increase in the pore radius, the concentrations of coions and counterions converge; therefore, the contribution of coions to the electric charge transfer increases. Reducing the number and/or radius of the pores leads to a decrease in conductivity [12,41] but can improve the membrane permselectivity. The relationship is a well-known trade-off between the membrane permeability and permselectivity and is

discussed in many recent reviews [27,57]. As for the effect of macropores on membrane transport characteristics, it can be taken into account using models that include a free solution phase, such as microheterogeneous, three-wire and cell models, which will be discussed below in Section 4.

The membrane conductivity increases with increasing water content [36]. At low water content, which can occur in a PEM of fuel cells due to water crossover [58], an increase in water content leads to a sharp increase in the percolation degree (see Figure 5c) causing an exponential growth in conductivity. At elevated water content, the higher w, the larger the pore size, which reduces the tortuosity of the inner membrane morphology, resulting in higher ion mobility.

3. Basics of Modeling of Ion and Water Transport in Ion-Exchange Membranes

The mathematical description of ion and water transport in membranes is reduced to several basic approaches [59–61], which include the balance and transport of charge and matter. In the following, we will briefly review the basic equations, present them in expanded and concise form, and discuss important aspects that will help formulate transfer problems in IEMs.

3.1. Conservation Equations

3.1.1. Material Conservation

Conservation equations form the main part of the fundamental basis for the mathematical description of mass transfer. Let us consider an elementary volume $\Delta V = \Delta x \Delta y \Delta z$ (Figure 8). The change in the amount of some substance in this volume over time t is due to two possible reasons. The first reason is the inequality of the incoming and outgoing fluxes of the substance (J_{sub}^{in} and J_{sub}^{out}, respectively). The second reason is the generation or decay of this substance inside the volume. Thus, the rate of change in the amount of a substance in an elementary volume is determined by the formula [62]:

$$\begin{pmatrix}\text{Substance amount}\\ \text{change rate}\end{pmatrix} = \left(\sum J_{sub}^{in} - \sum J_{sub}^{out}\right) + \begin{pmatrix}\text{Substance}\\ \text{generation rate}\end{pmatrix} - \begin{pmatrix}\text{Substance}\\ \text{decay rate}\end{pmatrix}. \quad (5)$$

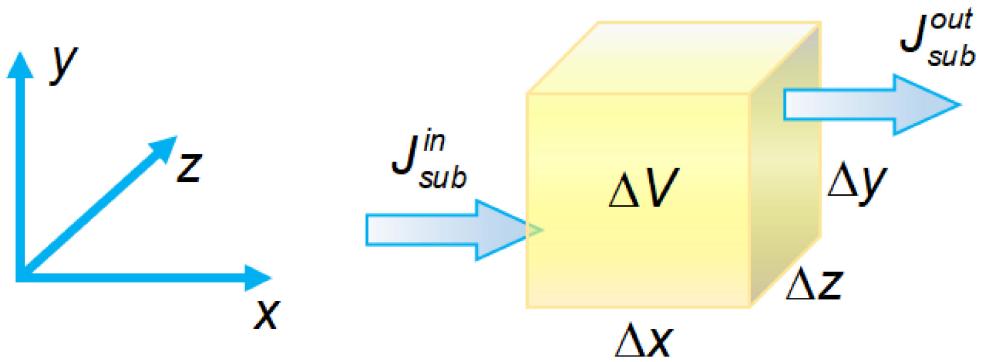

Figure 8. An elementary volume in three-dimensional space with incoming and outgoing fluxes of a substance.

In the mathematical description of the transport of species i (an ion or a molecule) in membrane systems, Equation (5) can be reduced to the following form [60]:

$$p^m \frac{\partial c_i}{\partial t} = -\left(\nabla \cdot \vec{j}_i\right) + p^m R_i, \quad (6)$$

where p^m is the pore volume fraction in the membrane; c_i (in mol/m^3 pore solution) and $\vec{j}_i$ (in mol/(m^{2}s) membrane area) are the concentration and the flux density of species i,

respectively; R_i (in mol/(m^{3}s) pore solution) is the generation rate of species i in a chemical reaction; and t is the time.

3.1.2. Navier–Stokes Equation

The Navier–Stokes equation is derived from the momentum conservation equation. This equation is based on Newton's second law of motion when considering all major surface and body forces acting on a unit fluid element. When a force is applied to this element, momentum is generated. Body forces, $\vec{F}$, are applied to the entire volume: the gravitational force is equal to $\rho\vec{g}\Delta V$, the electric body force is equal to $\rho_e\vec{E}\Delta V$, where ρ and ρ_e are the density and space charge density of the fluid, respectively; ΔV is the volume of the element; $\vec{g}$ is gravitational acceleration; and $\vec{E}$ is electric field intensity. Surface forces act on the surface of the body, including pressure (p), and friction force or internal stress (usually are taken into account using kinematic, ν, or dynamic viscosity,$\mu = \rho\nu$). The momentum conservation equation for a Newtonian fluid is written as follows:

$$\frac{\partial\rho\vec{v}}{\partial t} = -\vec{v}\cdot\nabla\rho\vec{v} - \nabla p + \mu\nabla^2\vec{v} + \vec{F}. \quad (7)$$

The term on the left-hand side of Equation (7) characterizes the rate of momentum accumulation per unit volume over time. On the right side, the first term describes the change in the convective component of the momentum flux entering and leaving the elementary volume. The second and third terms characterize the effect of the surface forces, the pressure and viscous forces, and the last term characterizes the effect of external body forces. In the case of IEMs, the gravity is often irrelevant and ignored.

Equation (7) is usually used in the models of fuel cells, where the gas phase is taken into account [30]. When a Newtonian incompressible fluid is considered, Equation (7) is reduced to:

$$\frac{\partial\vec{v}}{\partial t} = -(\vec{v}\cdot\nabla)\vec{v} - \frac{1}{\rho}\nabla p + \nu\nabla^2\vec{v} + \frac{1}{\rho}\vec{F}. \quad (8)$$

Equation (8) is largely applied when simulating solution flow between membranes in ED, RED and RedOx systems [23]. Sometimes the gravitational and electric body forces are important, which generate gravitational (natural) convection and electroconvection, respectively. In addition, Equation (8) is applied in the membrane pores, where electric body force can generate electroosmotic fluid transfer.

It should be noted that in the case of porous materials, where the gravity forces could be neglected, the empirical Darcy law is used instead the Navier–Stokes equation [63]:

$$\vec{v} = -\frac{k_P}{\mu}\nabla p, \quad (9)$$

where k_P is the hydraulic permeability of the porous medium.

3.1.3. Charge Conservation Law: Poisson Equation

The Poisson equation relates the distribution of an electric field with the distribution of space charge density:

$$\frac{\rho_e}{\varepsilon\varepsilon_0} = \nabla\cdot\vec{E} = -\nabla^2\varphi, \quad (10)$$

where ε_0 and ε are vacuum and relative permittivity, respectively; $\vec{E}$ is the electric field strength; and φ is the electric potential. This equation is important for modeling ion and water transport in membrane charged pores as well as when considering EDL in depleted solution near a membrane surface. The Poisson equation is based on Coulomb's law of electrostatics and its generalization, Gauss's flux theorem [64].

The charge conservation equation is an extension of the material conservation Equation (6). Multiplying it by the charge of species i, z_i, and the Faraday's constant, F, and summing over all species and noting that all reactions are charge balanced yields:

$$p^m \frac{\partial}{\partial t} F \sum_i z_i c_i = -\nabla F \sum_i z_i \vec{j}_i, \tag{11}$$

where the volumetric charge density, ρ_e, and the Faradaic current density, $\vec{i}_F$, can be defined by Equations (12) and (13), respectively:

$$\rho_e = F \sum_i z_i c_i \tag{12}$$

and

$$\vec{i}_F = F \sum_i z_i \vec{j}_i. \tag{13}$$

Combining the Poisson's (10) and charge conservation (11) equations gives the following equation for the current density [65,66]:

$$\vec{i} = F \sum_i z_i \vec{j}_i - \varepsilon\varepsilon_0 \frac{\partial \nabla \varphi}{\partial t} = \vec{i}_F - \varepsilon\varepsilon_0 \frac{\partial \nabla \varphi}{\partial t}. \tag{14}$$

The second term on the right-hand side of Equation (14) is the displacement current, which occurs due to very fast processes (lasting less than milliseconds), e.g., the high frequency part of the electrochemical impedance spectra [67]. In some cases, the contribution of the EDL charging/discharging process to the total resistance (or impedance) of the system is negligibly small compared with the contribution of other processes; thus, the second term in (14) may be neglected. The Faradaic current density, $\vec{i}_F$, does not change with distance (in the case of 1D geometry), while the total current density can change: a portion of the charges forming the current may be consumed, for example, by charging EDL.

Equation (14) should be applied to a continuous phase, which can be a solution in a membrane pore or outside the membrane, or a membrane itself considered as a homogeneous solution.

In some cases, the local electroneutrality (LEN) assumption may be applied:

$$\sum_i z_i c_i = 0. \tag{15}$$

This assumption can be applied to solution or bulk membrane except interfacial space charge regions (EDLs) [56]. Deviation from electroneutrality should be taken into account when describing transients and impedance spectra at small time scales or at high frequencies, when the double layer is charging and discharging, as well as when modeling length scales about the Debye length (on the order of nanometers) near the membrane surface. For these cases, Poisson's equation enables a correct description of the distribution and space charge density and electric potential/field strength [68].

The use of Equation (15) does not mean that the Laplace equation ($\nabla^2 \varphi = 0$) can be used to find the distribution of potential. The latter formally follows from Poisson's equation when $\rho_e = 0$ is substituted into Equation (10). Let us rewrite Equation (10) in the form:

$$C_+ - C_- = \widetilde{\varepsilon} \frac{d\widetilde{E}}{dX}, \; 0 \le X \le 1, \tag{16}$$

where $\widetilde{\varepsilon} = \frac{\varepsilon\varepsilon_0 RT}{F^2 c_s \delta^2}$, $X = \frac{x}{\delta}$, $\widetilde{E} = \frac{\vec{E}\delta F}{RT}$, and $C_i = \frac{|z_i| c_i}{|z_A| c_A}$ are the dimensionless permittivity, x coordinate, electric field strength and equivalent concentration of ion i, respectively; δ is the diffusion layer thickness; c_s is the molar concentration of salt in the electrolyte solution;

R is the gas constant; and T is temperature. The subscripts "+" and "−" correspond to the cation and anion, respectively; the subscript "A" corresponds to the coion.

The $\widetilde{\varepsilon}$ coefficient at the derivative in the right-hand side of Equation (16) is quite small. Therefore, the value of $\nabla^2\varphi$ (equal to $-\partial E/\partial x$ in a 1D case) may not necessarily be reduced to 0 to consider the value of $\sum_i z_i c_i$ to be approximately zero. Thus, Equation (15) can be applied out of the interfacial regions where j and E vary very rapidly with distance, causing a large value of $\nabla^2\varphi$. To find j and/or E in the regions where the LEN assumption is applied, Equation (15) should be solved together with the Nernst–Planck equations written for all mobile ions. This equation system can be considered as a simplification of the Nernst–Planck–Poisson (NPP) equation system [60]. The NPP equation system can be applied everywhere in membrane system. The limitations are related to the size of the considered region, which cannot be smaller than the size of atom/molecule [69].

Substitution of Equation (15) in (11) yields the following equation, showing that in the electroneutrality region, the divergence of the current density is zero (the current density does not change with a distance in the 1D geometry case):

$$\nabla \vec{i} = 0. \tag{17}$$

3.2. Irreversible Thermodynamics

Modeling ion and water transport in a membrane on the basis of the irreversible thermodynamics (the phenomenological approach) allows the establishment of general relationships between fluxes and driving forces that are valid for membranes of any type. This approach does not require an explicit description of the relationship between the membrane properties and its structure. On the one hand, this greatly simplifies the mathematical problem; on the other hand, important relations remain unknown. The peculiarities of ion and water transport in a particular membrane under study can be taken into account using phenomenological coefficients, which makes it possible to describe the membrane behavior under certain external conditions (concentrations, electric potential difference, solution flow rate etc.). To obtain quantitative relationships, it is necessary that the properties of the membrane be previously characterized. As a rule, such a description is sufficient for studying the patterns of development of various effects in electromembrane systems (e.g., concentration polarization and coupled transport phenomena, such as electroosmosis), for predicting energy consumption and current efficiency, and also for analyzing the applicability of membranes in specific applications. It should be noted that the equations used in the framework of the phenomenological approach may include phenomenological coefficients that directly or indirectly reflect the structural features of the membrane. For example, such coefficients can be evaluated via tortuosity factor, τ, used to take into account the fact that ion transport in the membrane is slower than in solution due to its dense structure [70–72]; membrane porosity, p^m, can be accounted for also to express the fact that ions and water can only pass through the pores of the membrane [30,73,74].

3.2.1. Onsager Phenomenological Equations

In a state of equilibrium, the electrochemical potential, μ_i, of any mobile species i is the same at every point of the membrane material. When the gradients of the electrochemical potential are not equal to zero, fluxes of species i appear in the system. Linear relationships between thermodynamic forces $\vec{F}_j = -\nabla\mu_i$ and the resulting fluxes $\vec{j}_i$ can be described by the Onsager equation:

$$\vec{j}_i = -\sum_j L_{ij}\nabla\mu_i, \tag{18}$$

where L_{ij} are the phenomenological conductivity coefficients. L_{ij} depend on the material properties, species concentration, temperature, and pressure. Note that generally the flux

of species i ($\vec{j}_i$) in Equation (18) depends not only on the thermodynamic force applied to that species ($\vec{F}_j$) but also on all forces acting on other species.

The electrochemical potential μ_i in Equation (18) can be represented as a function of activity a_i of species i, electric potential φ and pressure p in the virtual solution (an electroneutral solution that is in local equilibrium with a small membrane volume corresponding to the x coordinate [75]):

$$\mu_i = \mu_i^0 + RT \ln a_i + z_i F \varphi + \overline{V}_i p, \tag{19}$$

where μ_i^0 and $\overline{V}_i$ are the standard electrochemical potential and partial molar volume of species i, respectively.

Onsager's reciprocity theorem (1931) suggests that the matrix composed of the phenomenological coefficients is symmetric [59]:

$$L_{ij} = L_{ji}. \tag{20}$$

This relation makes it possible to reduce the number of independent phenomenological coefficients. For example, if three different species (counterion, coion, and solvent) are present in a membrane or solution, then the number of independent coefficients is six.

Along with the Onsager Equation (18), the relationship between the fluxes and forces can be expressed using other systems of equations (Spiegler, Stefan–Maxwell, Kedem–Katchalsky, and some others) [76–78]). Generally, these systems are mathematically equivalent, which allows moving from one system of equations to another by simple transformations of variables; at least it is possible in the case of Onsager and Kedem–Katchalsky equation systems [79].

3.2.2. Kedem–Katchalsky Equations

The Kedem–Katchalsky Equation system [76] is of great interest for the practical description of ions and water transport through membranes. In differential form, these equations are written as follows [79]:

$$\vec{j}_V = -L_p(\nabla p - \sigma RTc_s v_\pm \nabla \ln a_\pm) + \beta \vec{i} = -L_p(\nabla p - \sigma \nabla \pi) + \beta \vec{i}, \tag{21}$$

$$\vec{j}_i = -P\nabla c_i + \frac{\vec{i}\, t_i}{z_i F} - c_i L_p (1-\sigma)\nabla p, \tag{22}$$

$$\nabla \varphi = -\frac{\vec{i}}{\kappa} - \frac{RT}{F}\left(\frac{t_+}{z_+}\nabla \ln a_+ + \frac{t_-}{z_-}\nabla \ln a_- - \beta c_s v_\pm F \nabla \ln a_\pm\right) - \beta \nabla p, \tag{23}$$

where $\vec{j}_V$ is the volumetric flux density; L_p, β and P are the hydraulic, electroosmotic and diffusion permeability coefficients, respectively; π is the osmotic pressure; σ is the Staverman reflection coefficient (if $\sigma = 1$ then the membrane completely reflects the solute carried by the convective flow through the membrane; $\sigma = 0$ corresponds to zero solute reflection); c_s and c_i are the molar concentrations of salt and ion i, respectively, in the virtual solution of the membrane; $v_\pm = v_+ + v_-$ is stoichiometric number; $a_\pm$ is the average ionic activity of the electrolyte; t_i is the transport number of species i (equal to the fraction of electric current carried by ion i at zero concentration and pressure gradients); and κ is the electrical conductivity.

The fluxes described by Equations (21)–(23) are functions of three thermodynamic forces acting in the membrane system: mechanical, caused by the hydrostatic pressure gradient ∇p; electrical due to electrical potential gradient, $\nabla \varphi$; and chemical, expressed through the gradient of osmotic pressure or solute activity, coupled by the following relation [76]:

$$\nabla \pi = RTc_s v_\pm \nabla \ln a_\pm. \tag{24}$$

The transport coefficients L_p, β, P, t_i, κ and σ in the Kedem–Katchalsky equations are commonly used to characterize the transport properties of a membrane [14,80,81] and are called practical coefficients. Due to this, Equations (21)–(23) form the basis for the characterization of membranes and membrane processes [42]. The experimental measurement of such transport coefficients is carried out, as a rule, when only one driving force acts in the system. For example, to determine the diffusion permeability coefficient P, it is necessary to carry out measurements at $\nabla p = \vec{i} = 0$ [82–85].

3.2.3. Nernst–Planck Equation

The classical Nernst–Planck equation can be considered as a special reduction of the Onsager equation. If the cross-phenomenological coefficients in Equation (18) are neglected and Darcy's law (9) (establishing a linear relationship between the fluid flow velocity, $\vec{V}$, and pressure gradient) is applied, the extended Nernst–Planck equation with a convective term can be obtained [60]:

$$\vec{j}_i = -p^m D_i \left(g \nabla c_i + z_i c_i \frac{F}{RT} \nabla \varphi \right) + c_i \vec{V}, \tag{25}$$

where $D_i = \frac{L_i RT}{c_i}$ is the diffusion coefficient of species i; $g = 1 + \frac{d \ln \gamma_i}{d \ln c_i}$ is the activity factor; and γ_i is the activity coefficient of species i.

In some cases, it is convenient to apply in the membrane the ion transport equation in the reduced form, which could also be derived from Equation (25) using the LEN assumption (15) and Equation (13):

$$\vec{j}_i = -p^m D \nabla c_i + \frac{\vec{i}\, t_i}{z_i F} + c_i \vec{V}. \tag{26}$$

3.3. Chemical Reactions

Accounting for chemical reactions is necessary when considering the transfer of a weak electrolyte (water, ampholytes, etc.) [86] or a multicomponent solution whose species react with functional groups of the membrane or with each other (for example, in fuel cells) [30]. The protonation and deprotonation of weak acidic or basic functional groups [73,87,88] is of particular interest because they are a source or absorber of protons and hydroxyl ions but do not move in space and determine the selectivity of the membrane. In the case of bipolar membranes (BPM), the catalytic water splitting reaction occurs in the bipolar region [29] and in the membrane bulk.

3.4. Donnan Equilibrium Relation

The Donnan model and, in particular, relation (30) obtained in 1911 [46], can be considered as the first successful attempt to interpret the known experimental results on electrolyte sorption by a membrane. In this model, an ion-exchange material is considered as an ideal gel. The Donnan equilibrium between a solution and an ion exchanger is described by the continuity of electrochemical potential at their interface [37,60,61,89]:

$$RT \ln a_i + z_i F \varphi = RT \ln \bar{a}_i + z_i F \overline{\varphi}, \tag{27}$$

where the value with the overbar refers to the ion-exchanger.

The following two relations are derived from Equation (27). One is for the activities,

$$(\bar{a}_+^k)^{1/z_+} / (\bar{a}_-^k)^{1/z_-} = (a_+^k)^{1/z_+} / (a_-^k)^{1/z_-}, \tag{28}$$

and the other is for the electric potential difference between two phases (called the Donnan potential):

$$\Delta\varphi_D = \overline{\varphi}^k - \varphi^k = -\frac{RT}{z_+F}\ln\frac{\overline{a}_+^k}{a_+^k} = -\frac{RT}{z_-F}\ln\frac{\overline{a}_-^k}{a_-^k}, \quad (29)$$

where k is the left-hand (k = I) or right-hand (k = II) membrane/solution interface.

Taking into account that $a_i = c_i\gamma_i$ and $\overline{a}_i = \overline{c}_i\overline{\gamma}_i$, we find from Equation (29) the Donnan relation for a binary electrolyte:

$$\frac{(\overline{c}_+)^{1/z_+}}{(\overline{c}_-)^{1/z_-}} = K_D\frac{(c_+)^{1/z_+}}{(c_-)^{1/z_-}}, \quad (30)$$

where $K_D = (\gamma_\pm/\overline{\gamma}_\pm)^{1/z_+-1/z_-}$ is the Donnan equilibrium coefficient, expressed through the ratio of the mean ionic activity coefficients in the external solution, $\gamma_\pm = \left(\gamma_+^{\nu_+}\gamma_-^{\nu_-}\right)^{1/\nu} = \left(\gamma_+^{1/z_+}\gamma_-^{-1/z_-}\right)^{(1/z_+-1/z_-)^{-1}}$, and in the membrane, $\overline{\gamma}_\pm = \left(\overline{\gamma}_+^{\nu_+}\overline{\gamma}_-^{\nu_-}\right)^{1/\nu} = \left(\overline{\gamma}_+^{1/z_+}\overline{\gamma}_-^{-1/z_-}\right)^{(1/z_+-1/z_-)^{-1}}$. The electrolyte activity coefficients in aqueous solutions can be taken from the literature [90,91].

The Donnan theory cannot quantitatively predict the activity coefficients in the membrane. However, the consideration of only the "free" or "bulk" water in the membrane [92,93] makes it possible to achieve quantitative agreement between the theory and experimental coion sorption.

Another approach is to generalize the Donnan theory by taking into account the Manning condensation theory [94]. This approach is described in the next section.

3.5. Donnan–Manning Equilibrium Relation

3.5.1. Manning's Condensation Theory

Manning's model [95] has been a core element in the theoretical consideration of polyelectrolyte solutions since 1970s. The proposed equations have shown their applicability in a wide range of polyelectrolyte solutions [95,96] and are still successfully applied.

Manning's theory is based on the mean field approximation [95] and does not contain adjustable parameters. It takes into account only long-range point-to-line electrostatic forces, which cause "condensation of counterions" around charged polymer chains [95]. The theory is based on a simplified representation of the distribution of fixed charges in a polymer chain. The model is based on a dimensionless parameter, which is the reduced linear charge density of the polymer, ξ,

$$\xi = \frac{\lambda_B}{b} = \frac{e^2}{4\pi\varepsilon_0\varepsilon k_B T b}. \quad (31)$$

The critical value of this parameter is:

$$\xi_{\text{crit}} = \frac{1}{|z_Q z_c|}, \quad (32)$$

where λ_B is the Bjerrum length; b is the distance between two neighboring functional groups; e is the protonic charge; k_B is the Boltzmann constant; z_Q is the charge of the functional group; and z_c is the charge of the counterion. The value of ε was left as that of pure water because Manning's model considers dilute systems. The Bjerrum length represents the distance at which electrostatic forces between two elementary charges are comparable in magnitude to the thermal energy scale [97]. At a distance of less than $z_Q z_c\lambda_B$, the energy due to the electrostatic attractive force of a functional group (Figure 9a) prevails over the thermal energy. To diffuse away from the polymer chain, the counterion has to escape the attractive force of the fixed ions. Two neighboring fixed charges on

a polyelectrolyte chain, separated by a distance b, may have regions of predominating electrostatic influence (of radius $z_Q z_c \lambda_B$) which are overlapping (Figure 9b,c). The local energy minima created by the overlap results in the condensation of the counterions.

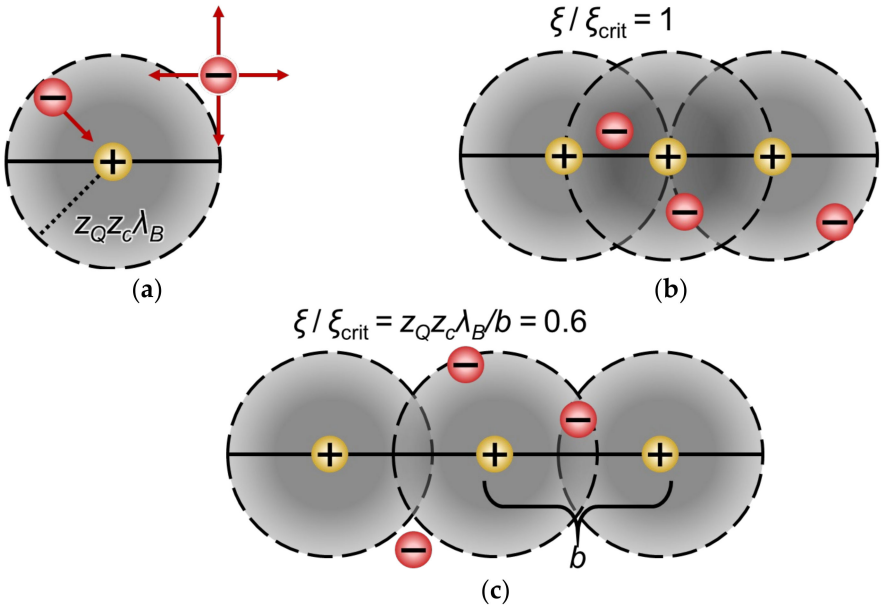

Figure 9. Schematic representation of the attraction of counterions by neighboring functional groups of a polyelectrolyte chain at different ξ/ξ_{crit}. (**a**): Within a distance of $z_Q z_c \lambda_B$ the counterions escape the attractive force of a fixed ion to diffuse away. (**b**): Region of adjacent electrostatic influence overlaps at the location of the fixed charges. (**c**): Region of adjacent electrostatic influence overlaps away from the fixed charge groups. Adapted from [98].

3.5.2. Condensation Theory Applied to IEMs: Donnan–Manning Theory

It is difficult to measure the average distance between functional groups, b, of an IEM. For a cross-linked IEM, b can be calculated from the theoretical or experimental ion-exchange capacity and knowledge of the membrane's molecular architecture [99]. Jang et al. [100] considered homogeneous gel membranes (not containing meso and macropores). For example, in the case vinyl polymers, the following equation was proposed:

$$b = 2.5\ \text{Å}\left(1 + \frac{n_{xl}}{n_{ch}}\right), \tag{33}$$

where n_{xl} is the mole fraction of neutral crosslinker and n_{ch} is the mole fraction of charged monomer; and 2.5 Å is the projection length of a repeat unit of vinyl polymers. The functional groups are assumed to be evenly distributed on the polymer backbone.

Authors [101–105] studied laboratory scale IEMs, whose structure was known quite accurately. This made it possible to calculate the value of parameter b. In a fairly wide range of electrolyte concentrations, good agreement was found between theoretical and experimental data on coion sorption. It should be noted that for the best agreement, the membranes should be as close to homogeneous as possible. The presence of inhomogeneities leads to the need to apply additional assumptions when determining b.

Determining the parameter b of commercial membranes is also not particularly difficult if the structure of their matrix is known [94,106,107]. However, in some cases, when the exact determination of b is difficult, ξ is treated as an adjustable parameter [108,109]. Even in this case, interesting observations may be made. In particular, the Neosepta IEMs of the latest generation (CSE and ASE) have larger values of ξ than the previous generation of these membranes (CMX and AMX), so counterion condensation is more significant in the case of CSE and ASE [110].

In the presence of large inhomogeneities (tenth of nanometers), such as in the case of the Nafion 117 membrane, the size and proportion of hydrophilic and hydrophobic regions (see Figure 4b) must be taken into account. From the point of view of the Donnan–Manning theory, such an IEM is heterogeneous. The use of various assumptions and/or ξ as an adjustable parameter makes it possible to achieve sufficient agreement between the theory and experiments on ion sorption [94,100,111,112]. Block copolymer electrolyte (BCE) phase-separated membranes are considered in [113,114]. These membranes also have inhomogeneities in the structure, but the structure parameters are known. The authors succeeded to predict b based only on the structure parameters of the charged half of the BCE.

In the case of commercial reverse osmosis (RO) membranes, consideration of the concentration of fixed ions in a dense active layer made it possible to determine b (with some assumptions) and predict the partition coefficients of RO membranes equilibrated with different chloride solutions (LiCl, NaCl, KCl, RbCl, and CsCl) [115,116].

The estimation of the dielectric constant, ε, is also complicated. The polymer can occupy more than half of the total membrane volume. As mentioned in Section 2, average dielectric constants in IEMs may be experimentally determined via microwave dielectric relaxation spectrometry (Figure 6) [48,105,117,118]. ε may be calculated using the co-continuous model [94,98]:

$$\varepsilon = \varepsilon_p(1 - \phi_w) + \varepsilon_w\phi_w, \quad (34)$$

where, ϕ_w is the membrane water volume fraction, and ε_p and ε_w are the polymer and water dielectric constants, respectively.

4. Modeling of Ion and Water Transport in IEMs

Most of the known mathematical models describing ion and water transport in charged membranes can be classified according to the scheme shown in Figure 10. All the models are conditionally divided in two types which differ in the approach to describing the structure-property relationship. In the first approach, used in the so called "solution-diffusion" models, the membrane material is considered as a quasi-homogeneous (macroscopically homogeneous) medium [119]. The components of the external solution are dissolved (sorbed) in this medium and can be transported there under the action of concentration, electric potential and pressure gradients. In "pore-flow" models, only one pore is considered. The transport of species here occurs under the action of the same driving forces as in the "solution-diffusion" models. The difference is that these forces are applied only in an aqueous solution phase filling the pore. The "pore-flow" models are also called "capillary" models (because they are based on the models previously developed to describe ion and water transport in capillaries), and "space charge" models (since it is essential to take into account the deviation from LEN in EDL formed at charged pore walls). The main governing equations relating species fluxes to driving forces (the Onsager, Kedem–Katchalsky or Nernst–Planck equations) are applied in both "solution-diffusion" and "pore-flow" models [120].

"Solution-diffusion" models have been developed for membranes considered as a single-phase medium or a multiphase medium. In the first case, the Teorell–Meyer–Sievers (TMS) model is most often used. In the second case, the effective medium approach [121] is applied. When formulating mathematical problems for some specific membranes/cases, various conditions/assumptions may be used. This may be the LEN assumption or the use of Poisson's equation in "solution-diffusion" models. Assumptions of infinitesimal or finite species sizes are used in "pore flow" models, while the use of Poisson's equation is almost always necessary because of the existence of a space charge in charged pores. Below we will consider in more detail the models that form the scheme in Figure 10.

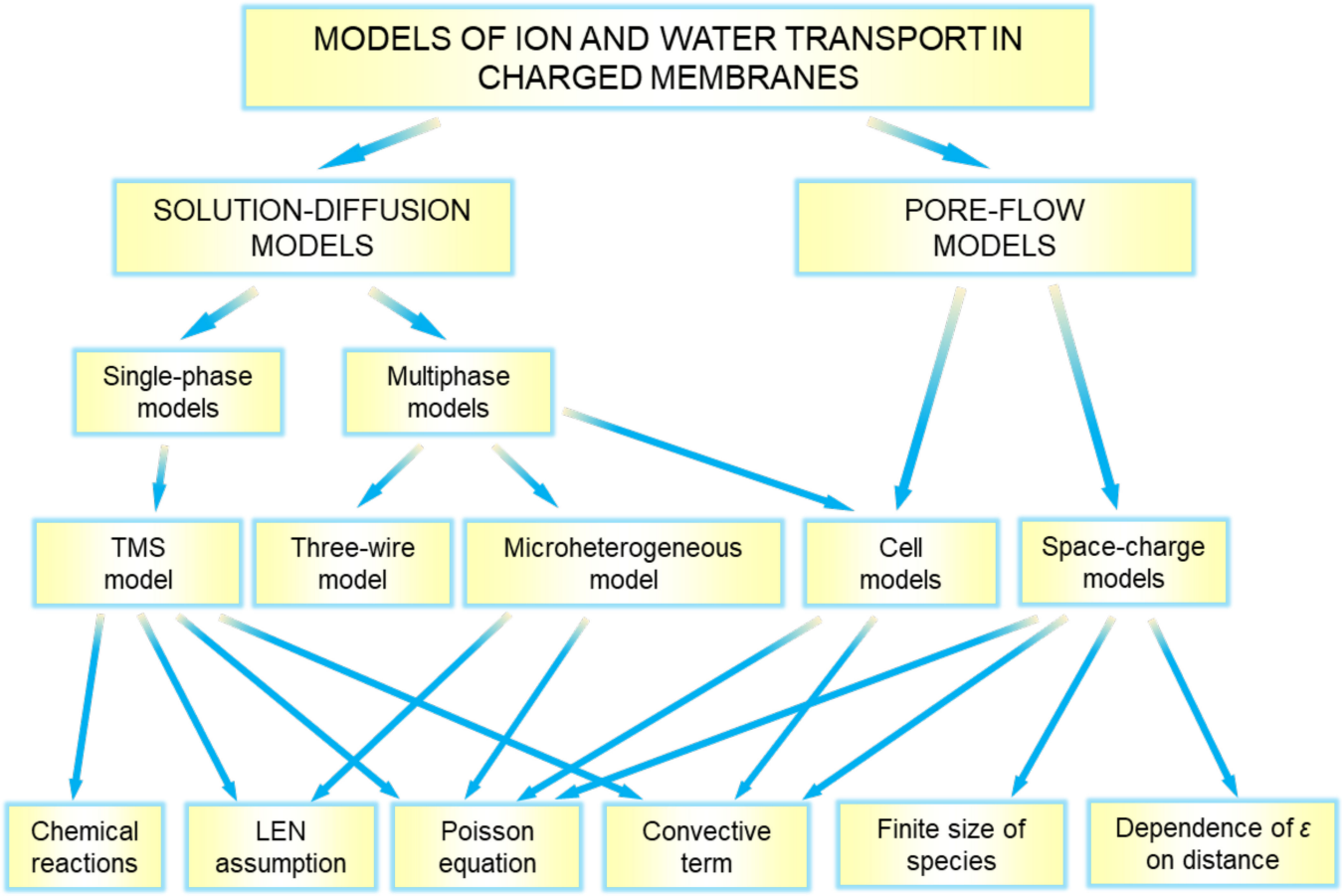

Figure 10. Classification of mathematical models used for describing ion and water transport in charged membranes.

4.1. "Solution-Diffusion" Models

4.1.1. Teorell–Meyer–Sievers (TMS) Model

The first successfully applied model for revealing the main properties of charged membranes was a model proposed independently by Theorell [122] and Meyer and Sievers [123] in the 1930s, called the TMS model [124]. It serves as the basis for the mathematical description of ion transport in IEMs when the "solution-diffusion" approach is used.

The TMS model is based on the Nernst–Planck equation (25). The membrane is considered as a single homogeneous phase (charged gel), or in other words, an aqueous solution of matrix polymer chains together with mobile ions and functional groups. The underlying model includes the assumption of LEN (15) in the membrane, an equation expressing electric current as the sum of individual ion flux densities (13), and the Donnan equilibrium relation (35) at the left-hand (I) and right-hand (II) interfaces used as the boundary conditions:

$$\frac{\left(\bar{c}_+^k\right)^{1/z_+}}{\left(\bar{c}_-^k\right)^{1/z_-}} = K_D \frac{\left(c_+^k\right)^{1/z_+}}{\left(c_-^k\right)^{1/z_-}},\ k = \mathrm{I},\ \mathrm{II}, \tag{35}$$

where $\bar{c}_i^k$ and c_i^k are the concentrations of ion i at interface k, from the side of the membrane and solution, respectively [37].

Equation (29) is also used for calculating the potential drop across the solution/membrane interfaces [125].

Instead of the LEN assumption (15) and Donnan equilibrium (35) at membrane boundaries, the Poisson Equation (10) can be used [126–128]. In this case the activity coefficients of each species are involved; in principle, they can be determined from the data in the

literature [90,91] or estimated using an appropriate theory such as Donnan–Manning [99] or others.

The TMS model gives an adequate qualitative description of such fundamental membrane properties as electric conductivity, transport number and membrane potential. When two kinds of counterions, 1 and 2, are present in the membrane, the Nernst–Planck equation together with Equations (29) and (35) enables the description of counterion competitive transfer. For more information on the TMS model, see references [59,129]. The paper [130] gives a description of the main features of this model and analyzes the area of its applicability.

Modeling of ion and water transport in systems with BPM is mainly carried out using the TMS model [73,131,132]. This is due to the fact that the processes in the interphase layer between the cation-exchange and anion-exchange layers, where the maximum electric field strength and the catalyst are located [133], are of the greatest interest, and the description of the processes of ion and water transport [134] in the membranes themselves should be, first of all, qualitative. The processes of energy accumulation and production [135–137] using BPM are also well described and predicted using the TMS theory. A recent paper [138] reveals that in the anion exchange layer of BPMs, the charge is carried mainly by bisulphate and sulphate ions instead of hydroxyls, produced inside BPM. The developed models make it possible to describe the current-voltage characteristics [70,73,139,140], the electrochemical impedance spectra [141] of BPM and asymmetric BPM, the performance of ED devices (using a 2D model [142]), and to explain the selectivity of IEMs with a modified surface in ternary electrolyte solutions [70,71,143,144]. Some software packages (e.g., COMSOL Multiphysics) include modules based on the TMS model and are used in modeling of such processes [70].

Using this simple approach, it is possible to explain the deviation of the IEM behavior from the classical one in solutions of weak electrolytes (such as phosphate or tartrate salts) and explain some features of this behavior compared with that in strong electrolyte solutions: the appearance of a second limiting current [145], increased diffusion permeability [74] or unusual concentration dependence of membrane conductivity [146]. Models based on TMS shed light on the transient characteristics of IEMs [128] and provide an explanation for scaling formation on surfaces in solutions with multivalence ions [147]. It is still an indispensable theoretical tool in the field of RED [148–151] and fuel cells [17,30,58]. It is applicable also in environmental analysis systems based on dialysis membranes [152]. In [153,154], the authors use the same assumption as the TMS model but apply the extended Nernst–Planck equation, which contains the convective term that is important when considering the application of IEMs in chlor-alkali electrolysis.

There are models considering the membrane as a single phase (charged gel), in which the concentration of fixed charges and/or diffusion coefficients continuously change along the normal coordinate [155,156]. Generally, these models show that a heterogeneity in the fixed charge distribution leads to an increase of permselectivity in comparison with a membrane wearing homogeneously distributed fixed charges of the same average concentration. The explanation is that the permselectivity is controlled by the layer with the highest local concentration of fixed charge, while the layers with low fixed charge concentrations have a minor impact on the global membrane behavior.

The further development of the TMS model could proceed in several ways. One is to apply other transport equations such as Stefan–Maxwell [30] and Kedem–Katchalsky [76] instead of Nernst–Planck. In addition, the Poisson equation could be used instead of the LEN assumption. However, the basic principle of representing the membrane structure remains the same: the membrane is considered as a single gel phase. Another approach takes into account inhomogeneities in the membrane structure, which can be at different levels from a few nanometers to microns. In the following subsections, we will discuss the models dealing with pores and clusters, as well as hydrophobic regions, which are revealed by experimental investigations.

4.1.2. Multiphase Models

In multiphase models a membrane, in accordance with the effective medium approach [121], is represented as a quasi-homogeneous system comprising two (or several) phases, the transport properties of which are functions of the properties of the corresponding phase [157,158]. This system may be considered as an array of capillary pores [159], a cluster-channel network [160], or as a uniformly distributed porous "grains" [161].

Microheterogeneous Model

Earlier, in Section 2, we mentioned that charged membranes are porous materials. The structure of these materials generally includes micro-, meso-, and macropores. To distinguish between these types of pores, one can use the ratio of the pore radius r to several characteristics, such as the EDL length, λ, or length of action of adsorption forces [162]. Usually, micropores are considered as the pores for which $r < \lambda$ (approximately, $r < 1.5$ nm). If $r > \lambda$, but r and λ are in the same order, then we are dealing with a mesopore; the condition $r >> \lambda$ ($r > 50$ nm) is characteristic of macropores. Mesopores and macropores contain an electrically neutral solution in their central part. Such a solution can be considered as a separate phase, and its properties (ion and water diffusion coefficients, permittivity) are very close to those of an external free solution equilibrated with the membrane [24].

Based on the above, the first phase can be distinguished in the IEM structure: an electrically neutral solution in meso- and macropores. Then the remaining volume can be attributed to the second phase. This second phase is the "gel phase" [157], which includes a hydrated polymer matrix with fixed charged groups whose charge is compensated by the charge of mobile ions. The gel phase can be considered as a microporous medium not containing electroneutral solution (Figure 7).

It is important to note that in reality, there is no distinct boundary between the intergel electroneutral solution and the EDL at the internal pore walls. Nevertheless, the conditional separation of the membrane material into different phases makes it possible to simplify the mathematical description. The main idea of such a model approach is to assign certain physicochemical properties to each phase. Then the properties of each individual phase are functionally related to the entire membrane properties (effective medium approach [121]).

Consider a macroscopic volume in the form of a layer of thickness dx (Figure 7). This layer should be sufficiently large to be "representative" and contain all membrane phases. At the same time, it should be small enough to be considered elementary when applying the transport equations in differential form, such as the Onsager Equation (18). Detailed changes in the concentrations and potential within dx are not considered, and the values of these parameters in phase elements are averaged; it is assumed that the phases in the dx layer are in equilibrium with each other. When describing ion and water transport, the problem is to obtain the effective transfer coefficient L_i, which characterizes the membrane layer of thickness dx as a function of L_i^k coefficients (characterizing the individual phases k), and the structural-geometric parameters characterizing the shape and mutual arrangement of the phases.

The first elements of the microheterogeneous model were formulated by Gnusin et al. [163] when developing the so called "principle of generalized conductivity", which is an analog of effective medium theory [121]. The main elements of this model and its experimental verification are described in [157,164]. Later, some modifications of this model [39,165–167] and numerous applications are presented in [14,28,39,165–178]. The application of the microheterogeneous model allows, along with the electrical conductivity of the membrane [168,170–173,177,178], the determination of electrolyte diffusion permeability [14,21], permselectivity (ion transport numbers) [14,21,28,174,179], electrolyte sorption [180–182] and some other properties [14,21,176,183]. It is possible to quantitatively describe the concentration dependences of the mentioned membrane characteristics based on a single set of structural and kinetic parameters [14,21,176].

Within the framework of the microheterogeneous model, the transport equation is written in a form reduced from the Onsager Equation (18).

The effective membrane conductance coefficient L_i is then expressed as follows [157]:

$$L_i = \left[f_1 \left(L_i^g \right)^{\alpha} + f_2 (L_i^s)^{\alpha} \right]^{1/\alpha}, \quad (36)$$

where L_i^g refers to the gel phase, and L_i^s to the intergel electroneutral solution; f_1 and f_2 are the volume fractions of the corresponding phases $f_1 = V_g/V_m, f_2 = V_s/V_m, f_1 + f_2 = 1$ (where V_g, vs. and V_m are the volumes of gel, intergel solution and the membrane, respectively); and α is the structural parameter depending on the position of the phases with respect to the transport axis (when the phases are parallel to this axis, $\alpha = 1$; when they are in serial disposition, $\alpha = -1$; and in other cases $-1 < \alpha < 1$).

The mathematical description of the ion transport in the gel phase contains all the assumptions made in the TMS model (see Section 4.1.1). The properties of the intergel solution are the same as those of the equilibrium bathing solution. The Nernst–Planck equation (Equation (25) without a convective term) is used, and the condition of local electrical neutrality (Equation (15)) is assumed. L_i^s and L_i^g are expressed as functions of the ion diffusion coefficients, D_i^s and D_i^g, and the concentrations, c_i^s and c_i^g, in the corresponding phases [157]:

$$L_i^s = D_i^s c_i^s / RT, \; L_i^g = D_i^g c_i^g / RT. \quad (37)$$

Concentrations c_i^s and c_i^g are linked by the Donnan relations (Equation (30)), the local equilibrium being assumed between both phases.

As a rule, IEMs have a rather high concentration of fixed ions ($\overline{Q}$), close to 1 mol/L swollen membrane or higher. Therefore, in the case of dilute solutions, the concentration of coions in the gel phase is negligible compared with $\overline{Q}$. When assuming $\overline{c}_- << \overline{Q}$ and $\overline{c}_+ \approx \overline{Q}$, Equation (30) can be simplified. In the case of a symmetrical electrolyte ($z_+ = -z_- = z$) one obtains [56]:

$$\overline{c}_A = \frac{K_D^z}{\overline{Q}} c_A^2, \; \overline{c}_c = \overline{Q} + \overline{c}_A, \quad (38)$$

where the subscripts "c" and "A" refer to the counterion and coion, respectively; and c_A is the coion concentration in the intergel solution.

Since ions are present in both phases, the partition coefficient, K_s, involving the coion concentration in the membrane, c_A^*, can be found using Equation (38) [157]:

$$K_s = \frac{c_A^*}{c_A} = f_1 \frac{K_D}{Q^g} c_A + f_2. \quad (39)$$

The first and second terms on the right-hand side of Equation (39) correspond to the contribution of the gel phase and the intergel solution, respectively. Q^g and K_D are the ion-exchange capacity of the gel phase and the Donnan coefficient, respectively. Despite the fact that the intergel phase volume fraction in IEM is quite small (less than 0.1 in homogeneous membranes and about 0.2 in heterogeneous ones), the electrolyte is predominantly sorbed by this phase (especially in dilute solutions).

Equation (39) describes the linear dependence between K_s and the external solution concentration. At a low electrolyte concentration, K_s is close to f_2, i.e., its value is approximately 0.1 (or lower) for homogeneous membranes and about 0.2 for heterogeneous ones [56].

In the case of a binary electrolyte, the microheterogeneous model expressed by Equations (36)–(39) includes six basic input parameters: two static, K_D and Q^g (thermodynamics coefficients); two structural, f_1 and α; and two kinetic ones (D_1^g and D_A^g, diffusion coefficients in the gel phase). When these parameters are known, L_i coefficients can be calculated. The membrane transport characteristics (conductivity, κ, ion transport numbers,

t_i, and diffusion permeability, P) are calculated using equations relating the Onsager and Kedem–Katchalsky conductance coefficients:

$$\kappa = \left(z_+^2 L_+ + z_-^2 L_-\right) F^2, \tag{40}$$

$$t_i = \frac{z_i^2 L_i}{z_+^2 L_+ + z_-^2 L_-} = \frac{z_i^2 L_i F^2}{\kappa},\ i = +, -, \tag{41}$$

$$P = \frac{(z_+ L_+ t_- + |z_-| L_- t_+) RT}{c} = \frac{2RT\kappa t_+ t_-}{F^2 c}, \tag{42}$$

where $c = |z_i| c_i$ is the equivalent electrolyte concentration in the solution in equilibrium with the membrane.

It is important to note that Equations (40)–(42) are applicable both in the case where the membrane is in equilibrium with an external solution and in the presence of a concentration gradient across the membrane (zero or non-zero current). When there is a concentration gradient, Equations (40)–(42) are applied locally [56].

The input parameters of the microheterogeneous model (the six parameters listed above) are found from the experimentally obtained membrane exchange capacity and concentration dependences of electrical conductivity, and diffusion permeability. For example, the volume fraction of the gel phase (or intergel solution) can be approximately found from the concentration dependence of the membrane conductivity, κ [14,21,157,175,176,184]:

$$\kappa = (\kappa^g)^{f_1} (\kappa^s)^{f_2}. \tag{43}$$

Equation (43) is obtained as a limiting case of Equations (36) and (40) at $\alpha \to 0$.

At low electrolyte concentrations (usually < 1 M), the gel conductivity, κ^g, is almost independent of the electrolyte concentration due to the weak coion sorption by this phase. In this case, the dependence $\lg\kappa - \lg\kappa^s$, according to Equation (43), is linear with a slope factor f_2. According to numerical calculations, Equation (43) is held near the "isoconductance point" (where $\kappa = \kappa^g = \kappa^s$) if $|\alpha| \leq 0.2$.

A detailed algorithm for determining the remaining parameters of the microheterogeneous model is described in Reference [184].

Various modifications of the microheterogeneous model are also known [39,165–167].

Porozhnyy et al. [165] proposed a mathematical description of the effect of charged nanoparticles on the membrane transport properties. In addition to the gel phase and the electrically neutral solution, the presence of nanoparticles was considered (Figure 11). The core of the nanoparticle is impermeable to ions and water, but the EDL formed around it contributes to a significant increase in the counterion concentration in the pore solution. The fraction of the charged solution in membrane pores increases and the fraction of electroneutral solution decreases. As a consequence, the presence of charged nanoparticles causes an increase in the conductivity and a decrease in the diffusion permeability of the membrane [165]. According to Equation (42), these changes in κ and P result in an improvement in the membrane permselectivity with respect to counterions (an increase in the counterion transport number).

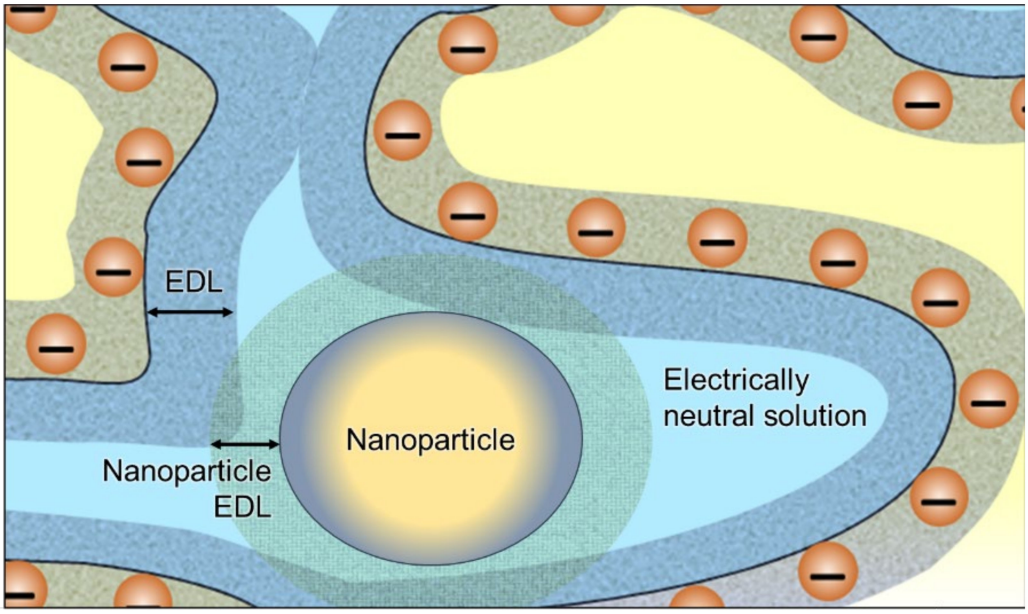

Figure 11. Schematic representation of a fragment of a mesoporous IEM containing a charged nanoparticle surrounded by an EDL. Redrawn from [165].

Nichka et al. [166] proposed a modification of the microheterogeneous model that takes into account the changes in the EDL thickness at the boundaries between the gel phase and the internal electroneutral solution, which occur with external concentration changes. This modification assumes that the EDL thickness at the pore wall increases with the dilution of the external solution inversely proportional to $\sqrt{c}$. As a result, the membrane conductivity decreases with solution dilution less rapidly compared with the basic version [157]. This trend agrees with experimental data [166].

Kozmai et al. [39] found the ion diffusion coefficients in the membrane gel phase, $\overline{D}_i$, and the volume fraction of the intergel phase, f_2, as functions of the membrane water content (the higher the water content, the higher $\overline{D}_i$ and f_2). The approach proposed in [39] made it possible to more correctly describe the transport characteristics of MA-40 and MA-41 membranes depending on the concentration and pH of the external solution. In this description, it was taken into account that the membrane water content decreases when the external concentration increases and when there is a loss in the exchange capacity. The latter is due to deprotonation of weakly basic fixed groups with increasing pH.

In another work of the same scientific group [167], the microheterogeneous model was supplemented to describe changes in the structure of the CJMA-7 anion-exchange membrane transport properties (Hefei Chemjoy Polymer Materials Co. Ltd., China) due to various modifications. The model [167] takes into account the presence of a perfluorosulfonated ionomer-modifying film on the substrate membrane surface and partial filling of macropores with this modifier. Salmeron-Sanchez et al. [175] applied the microheterogeneous model to describe the changes in transport-structural parameters of some anion-exchange and cation-exchange membranes caused by their modification with polypyrrole.

Three-Wire Model

Another approach was developed in the middle 1950s by Willie and Southwick [185]. The model described the system "ion-exchange resin particles/electrolyte solution" [186,187]. Later this idea was applied to ion-exchange membranes [188,189]. The model represents the system under study in the form of three parallel conducting layers [185,187] (Figure 12). The first layer consists of an electrolyte solution and ion-exchange gel arranged in series. It represents the passage of ions through the conductive spheres and the solution between them. The second layer is a pure ion-exchange gel. It describes gel phases (ion-exchange

granules in original work), which touch each other to form conducting paths. The third layer is the pure electrolyte solution. This component represents the conductance through the solution-filled regions (macropores in a heterogeneous membrane).

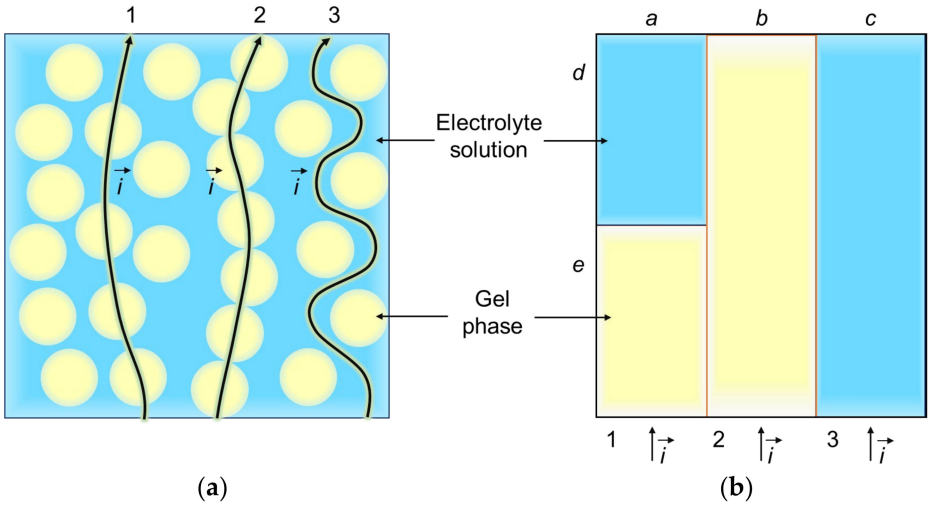

Figure 12. Schematic representation of three pathways of ions and electrical current in two-phase system (**a**) and three-wire model (**b**).

The resulting conductivity of the IEM κ_m is a function of the electrical conductivity of the gel phase κ_g and geometrical parameters a, b, c, d, and e of the model (Figure 12):

$$\kappa = a\kappa^g/(e + d\kappa^g) + b\kappa^g + c. \quad (44)$$

There are two relations between the geometrical parameters: $a + b + c = 1$ and $d + e = 1$. Thus, the number of independent fitting parameters can be reduced to three. Although the model has been proposed for a long time, it continues to be effectively used [158,174,190].

Cell Model

Filippov et al. [191–193] described the ion and water transport in IEMs using the so-called "cell method" proposed by Happel and Brenner [194]. The method is quite efficient for description of concentrated disperse systems. In the case of IEMs, cell models take into account the size and some transport properties (such as conductivity, hydraulic and diffusion permeability) of grains or fibers forming the system, as well as their packing patterns [195,196]. The macropores are formed between the grains (e.g., of an ion exchanger) packed into an array, and the micro- and mesopores concentrated in the grains themselves, are taken into account. Figure 13 shows an example of a membrane structure in the framework of cell models [197]. An IEM is presented as a periodic array of identical charged porous spheres (or cylinders) of radius a enclosed by liquid spherical (or coaxial) shells of external radius b instead of randomly distributed ion exchange clusters of different sizes. The sphere-to-cell (or cylinder-to-cell) volume ratio is equal to its total fraction in the disperse system.

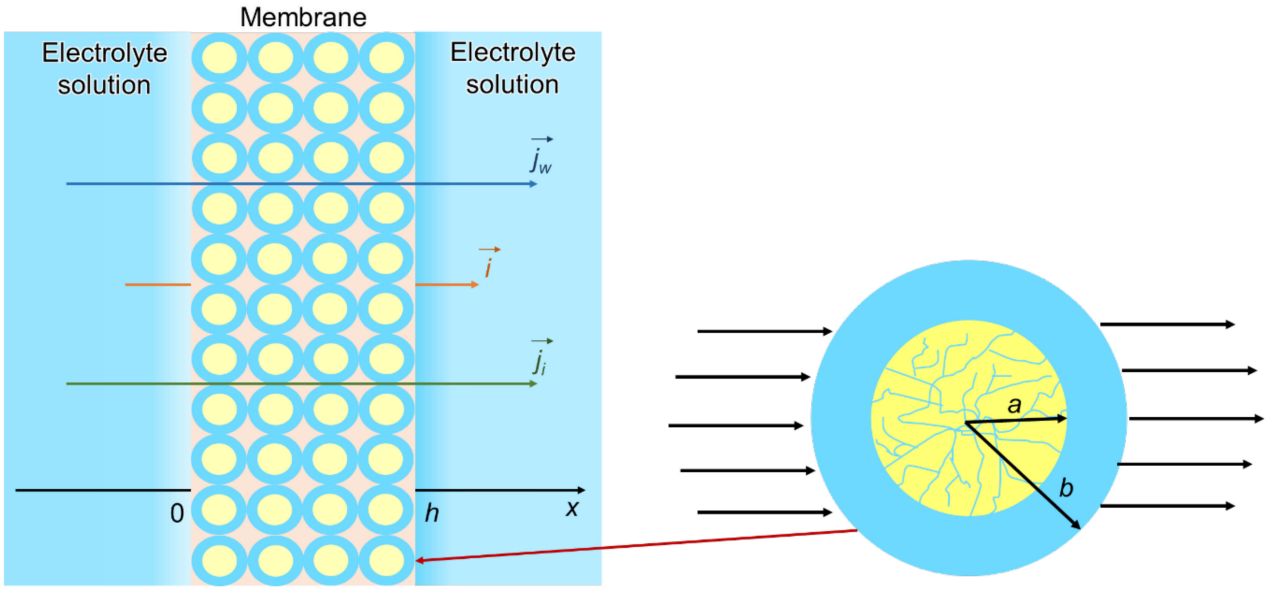

Figure 13. Schematic representation of a cell model, as described by Vasin et al. [197].

The mathematical formulation of the problem in the case of modeling membrane electric and hydraulic permeability has been presented in [161,196,198]. The extended Stokes Equation (8), taking into account the spatial electric force, describes a "creeping flow" (small Reynolds number) in the outer region of the sphere ($a < r < b$), and the Brinkman vector differential equation [199] with the spatial electric force describes the fluid transport in the inner region ($0 \leq r < a$). The Nernst–Planck equation with the convective term (25) coupled with the Poisson equation (10) is used for describing the ion flux density [196]. The mutual influence of adjacent particles is taken into account by establishing certain boundary conditions on their surfaces. An exact algebraic equation for the estimation of membrane hydrodynamic permeability was derived [161,196]. The correctness of the theoretical results was confirmed by their satisfactory agreement with the experimental data on the electrical conductivity and electroosmotic permeability of the MF-4SC cation-exchange membrane in various 1:1 electrolyte solutions [200]. In [201] the analytical expressions for conductivity, limiting current density and diffusion permeability for bi-layer IEMs were also in good agreement with the experimental data for membranes modified by polyaniline decorated clay nanotubes.

The cell method allows one to take into account different features of membranes. In [202], the action of surface forces on the walls of the micro- and mesopores is taken into account by stress jump at the fluid–porous interface. The authors [202] also considered the deformation of the shape of grains or fibers in the swollen state (deviation from the ideal spherical or cylindrical shape) to describe mass transfer through polymer membranes. In [203], the effect of an external magnetic field on the filtration of an electrolyte solution was considered. In [161], mathematical modeling of the electrobaromembrane process made it possible to confirm the conclusion made in previous experimental and theoretical studies [204,205]: the selectivity to equally charged ions may be achieved by the difference in their mobility resulting from a certain combination of potential and pressure difference applied to the membrane.

4.2. "Pore-Flow" Models

The "pore-flow" models describe the ion and water transport in a membrane pore [119,206], which is considered as a conducting channel (usually tubular). This approach originates from the description of ion and water transport inside microcapillaries with charged walls [120,207]. These models make it possible to describe such electrokinetic phenomena as the current-induced

transfer of a liquid relative to a charged solid surface or the transfer of charged solid particles in a liquid [208,209]. The main role in these phenomena is played by the EDL at the charged surfaces.

These kinds of models are often called "space-charge models" in the literature [210–214]. The ion and water transport are described by Nernst–Planck–Poisson–Navier–Stokes equation systems. The pore size and wall charge density are the main parameters characterizing the system [215].

The basic version of a space-charge model deals with a tubular pore (schematically shown in Figure 14) with surface charge on the walls. The model is based on the extended Nernst–Planck equation containing the convective term, Equation (25), written in 2D or 3D geometry with axis symmetry. The diffusion coefficients are usually assumed to be the same as in free solution. The cross-sectional distribution of local concentration is well described by the Poisson–Boltzmann equation. The fluid flow is described by the Navier–Stokes equation (8) with and electrical body force term [204]. The latter is provided by the tangential electric field applied to the space charge in the EDL. The walls are usually considered as uniformly charged. The impact of a non-uniform distribution of the pore wall charge on nanofiltration (NF) performance has been investigated by the group of Szymczyk in references [211,216,217]. In addition to NF, the condition of non-uniform pore wall charge distribution is used to describe the transport of ions and water in nanochannels in various other applications [218–222]. The potential at the pore walls may also be controlled using specially designed membranes [223,224] by applying an external voltage source. This makes it possible to switch the ionic selectivity of membranes so that a membrane can be a cation-exchange at one applied voltage, and an anion-exchange at another voltage [225,226].

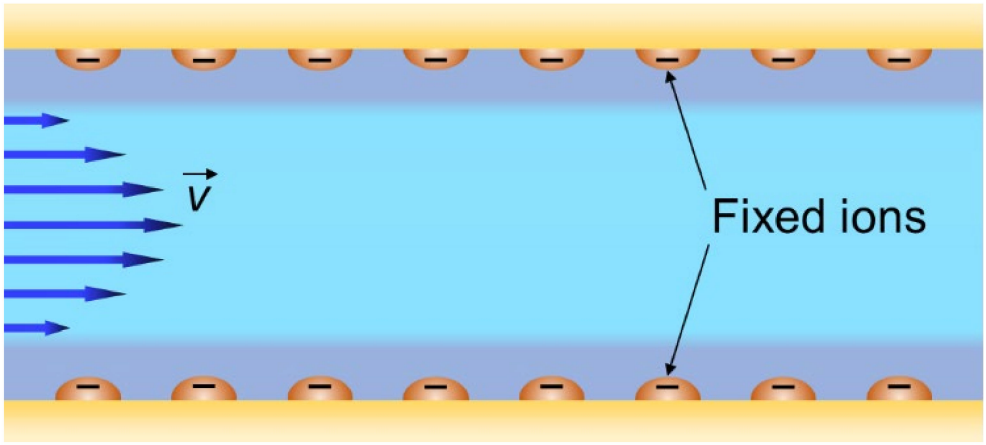

Figure 14. Schematic representation of solution flow in a tubular pore with charged walls; an EDL at the wall is shown in a darker shade. Redrawn from [52].

A simplification of the pore-flow model is possible in the case of the pores that are thin relative to the Debye length. The concentration profiles change only slightly across thin pores, as well as the potential [227]. This simplification is known as the "fine capillary pore model" or "uniform potential model". It also may be considered as an extended version of the TMS model [150], which takes into account the fluid flow.

Different versions of "pore-flow" models account for different effects at the interphases: the dependence of the dielectric constant on the distance from the pore wall [228], finite sizes of ions, ion hydration effects [229], adsorption of diluted species [210,230] and others [231,232]. These effects have a significant impact on the streaming potential [233], diffusion permeability [211] and permselectivity [234], pore conductivity [207,235] and some other properties, which can be computed using such models. These models are very useful for describing the ion and fluid transport in and around nanometer-sized objects with at least one characteristic dimension below 100 nm [236]. Bazant et al. [209,237] paid attention to the steric effects near a non-permeable wall at high voltages taking into account that solvated counter-ions are crowded there.

Cwirko and Carbonell [238] and later on Szymczyk et al. [239] have calculated using space-charge models the macroscopic Onsager's L_{ij} coefficients for a Nafion membrane as functions of the membrane nanostructure parameters (which are the pore radius, pore wall charge density and the tortuosity factor). Their comparison with the experimental coefficients determined by Narebska et al. [240] has shown a rather good agreement. Thus, it becomes possible to bridge the gap between two different approaches, i.e., the microscopic model description and the "solution-diffusion" models applied together with irreversible thermodynamics.

The "pore-flow" models can be applied not only to tubular pores, but also to pores with other geometries. Moreover, Balannec et al. studied how the geometry of a pore affects its permselectivity [217]. They found that hourglass-shaped nanopores in nanofiltration membranes improve their salt rejection. The explanation of this effect is that the filtration and desalination properties of hourglass-shaped nanopores are based on two different phenomena: the exclusion of coions in the thinnest region of the pore, and the magnitude of the pressure-induced electric field driving ions through nanopores. This interesting conclusion about the role of the shape of nanopores was proved experimentally [241,242].

5. Current State of Modeling of Ion and Water Transport in Membrane Energy Generation Systems

The previous section presents the main general approaches to the mathematical description of ion and water transport across membranes. However, questions remain about which of these approaches are most often used and how they are used in the case of membrane processes of energy generation. In this section, we analyze the current state of modeling in this field and consider in more detail examples of the description of ion and water transport in the RED and proton-exchange membrane fuel cells (PEMFC). It is important to note that for such processes, the "solution-diffusion" models are mainly used. This does not mean that "pore-flow" models are not applicable to such cases. However, modeling the distribution of ions in EDL is overly complex, although in the case of RED and PEMFC, convective transport within the membrane pores is not dominant.

5.1. PEMFC Models

In recent decades, hundreds of papers have been published on the simulation of PEMFC, which have been considered and structured by many comprehensive reviews [30,58,243–247].

The membrane in a PEMFC acts as a barrier to gas transfer, preventing mixing of H_2 and O_2 and electronic conduction between the anode and cathode, but acts as an ionic conductor, transporting H^+ protons in the form of hydronium ions H_3O^+ or $H_5O_2^+$. As described in Section 2, in the presence of water, a cluster-channel system is formed in the membrane, which provides ionic conductivity. The proton conductivity depends on the size of the clusters and especially on the channels. The latter is a strong function of water content. Therefore, the models describing the functioning of PEMFCs usually take into account the dependence of membrane properties on the water content and describe water transfer simultaneously with proton transfer.

Vapor equilibrated (VE) or liquid equilibrated (LE) conditions influence the water and proton transfer in the membrane and the interfacial resistance. PEMFCs are mostly operated under VE conditions at both electrodes, and PEM water electrolyzers for water splitting are mostly operated under LE [248]. Therefore, the PEM water content is rather low when the membrane is used in fuel cells, whereas it is high when operating in water electrolyzers. The humidity of PEM also determines the operating temperature of the PEMFC itself [249]: when the membrane dehydrates, its ionic resistance increases, which leads to an increase in its temperature and the temperature of the entire device. The water content in PEMs depends on the supply of water vapor from the supplied air to the cathode channel and on the transport of water formed in the porous electrode, where Reaction (4) takes place. The ionic conductivity of the membrane depends on the percolation effect (described in Section 2), which depends on the water content of the membrane. Thus,

water transport limits the performance of the fuel cell. Great attention is paid to water management, that is the optimization of water transport and water content in PEMFC [250].

In recent works on PEMFC models [250–258], a membrane is considered as a homogeneous phase in which water and proton transport occurs. The water flux through the membrane is described phenomenologically as the sum of two terms: a Fickian diffusion and an electroosmotic drag. Ion transport is taken into account through ionic conductivity (which is a strong function of water content and temperature) and current density.

In Section 2, we considered two mechanisms of proton transport in a PEM: the vehicle mechanism, in which protons are carried in the form of hydronium ions, H_3O^+ or $H_5O_2^+$; and the hopping (Grotthuss) mechanism, which is rather characteristic of bulk liquid water. Membranes at low hydration do not contain fluid domains with extensive hydrogen bond networks, the Grotthuss mechanism is suppressed, and the vehicle mechanism is considered to be dominant [24,111]. Launching the hopping mechanism at a higher water content, especially in LE conditions, increases the membrane conductivity.

In the field of fuel cell modeling, the most common approaches are those developed by Springer, Zawodzinski and Gottesfeld [259] (hereafter the "Springer model") and by Weber and Newman [260].

The widely used Springer model accounts for electroosmotic drag and water diffusion in the membrane in an essentially empirical manner. It considers a PEM under VE conditions only. The water content (in H_2O/SO_3^-), λ_w, in a Nafion 1100 PEM at the interface with the electrode as a function of water vapor activity outside the membrane, a_w, is presented as an empirical polynomial relation [259]:

$$\lambda_w = 0.043 + 17.81a_w - 39.85a_w^2 + 36.0a_w^3, \text{ at } 0 \leq a_w \leq 1. \quad (45)$$

A local equilibrium is assumed between the water vapor outside the membrane and the water content inside the membrane at the interface. The water vapor activity is calculated as $a_w = x_w P/P_{sat}$, where x_w and P are the mole fraction of water in the gas and the pressure at the electrode/membrane interface, respectively; P_{sat} is the saturation pressure of water. In the literature, the isotherm measured by Zawodzinski et al. [261] and expressed by Equation (45) is commonly used when modeling PEMFC [58,250,252,257,262] and PEM electrolyzers [248]. Nafion 1100 is the most popular PEM for which empirical sorption isotherms have been established experimentally [111].

The Springer model also includes the water diffusion coefficient measured by Zawodzinski et al. using the nuclear magnetic resonance method [261]. The application of Equation (45) at the left-hand and right-hand membrane sides allows calculation of the gradient of water content inside the membrane. When this gradient and the water diffusion coefficient are known, it is possible to find the distribution of water content within the membrane and the water flux. The local electrical conductivity of PEM is assumed to be a linear function of λ_w:

$$\kappa = a\lambda_w + b, \quad (46)$$

where the coefficients a and b depend on the temperature. These dependences for a given PEM are found experimentally. Then, when the water activities to the left and to the right of the membrane are known and an electric current density is given, Equations (45) and (46) together with Ohm's law make it possible to calculate the water flux and the potential drop across the membrane.

From a thermodynamic point of view, taking into account the pressure drop inside the membrane is most likely useful only under LE conditions [259,260]. The models that take into account the pressure gradient become relevant only in the LE mode when free liquid water is present in the PEM [260].

The main difference between the Springer model and the Weber–Newman model [260] is that the latter takes into account an additional effect. The Springer model accounts for water diffusion and water electroosmotic drag (when an electric current of protons induces water transport), and the ionic transport is assumed to depend only on the membrane

water content. The Weber–Newman model also considers another cross effect: water flux can induce a streaming current of protons. The latter effect is especially important under LE conditions.

The earlier models [259,260] have become widespread and have been supplemented with various empirical dependencies that refine water content, diffusivity, and ionic conductivity. The heat management is also quite important [250]. Machine learning processes are actively used on experimental data and calculation results using 3D models [244,263].

The developed approaches to describing the processes of proton and water transfer in a PEM consider the membrane as homogeneous. From the point of view of the classification given in Section 4, these models can be attributed to the "solution-diffusion" approach, namely, these models can be considered as special versions of the TMS model. Indeed, the Springer model, the Weber–Newman model and subsequent models take into account water transport and some coupled effects, such as electroosmosis and streaming current, which were not considered in the TMS model. In addition, as in the TMS model, a local equilibrium is postulated at the membrane/bathing solution (or vapor), but this equilibrium refers to water activities, and not to ion concentrations as does the Donnan relation used in the TMS model. The latter is not needed when modeling the PEMFC and the PEM electrolyzers since the presence of coions in PEMs is negligeable.

It has been found that when a PEM (such as Nafion 1100) is properly characterized experimentally, and the coefficients involved in the dependencies such as in Equations (45) and (46) are determined, a Springer-type model provides a good qualitative and quantitative description of the transport processes in this membrane. Moreover, the entire operation of the fuel cell can be quantitively described, which is important for practice.

At the same time, the fact that the description of ion and water transport through a PEM is carried out using empirical relationships, makes such a description too strongly tied to experiment. Such a description does not allow one to predict in advance how suitable a given membrane will be for operation in a fuel cell. It is necessary to develop models which use the theoretical structure-property relationships, namely, the dependencies of the internal water content on the water vapor activity outside the membrane as well as the dependence of the membrane proton conductivity on the water content.

5.2. RED Models

When describing the RED, attention is mainly paid to ion transport, while water transport is generally not important in this process. This is due to the fact that the main driving force is the ion concentration gradient, which weakly depends on the electroosmotic and osmotic water transport. In addition, these two contributions to water transport in the case of RED are counter-directional.

Veerman et al. [15] were among the first to take into account the features of transport phenomena in IEMs when modeling the RED process. Ionic fluxes in the membrane were described by the Nernst–Planck equation (25) in the approximation of a linear concentration distribution; the variation of ion concentration in the solution diffusion layers were not taken into account. The use of species conservation equations together with the fluxes found using the Nernst–Planck equations allowed calculation of the ion concentration distribution along the length of the membranes in chambers with sea water and river water flowing between a cation-exchange and an anion-exchange membrane. Along with the salt flux, j_{salt} (Equation (47)), the water flux, j_{water} (Equation (48)), due to osmosis of water from the river water compartment to the sea water compartment, was also considered:

$$j_{salt}(y) = \frac{i(y)}{F} + \frac{2D}{d}\left(c^S(y) - c^R(y)\right), \tag{47}$$

$$j_{water}(y) = -\frac{2D_{water}}{d}\left(c^S(y) - c^R(y)\right)\frac{M_{water}}{\rho_{water}}, \tag{48}$$

where y is the tangential coordinate; i is the current density; d is the membrane thickness; D and D_{water} are the membrane permeabilities towards the electrolyte and water, respectively; c^S and c^R are electrolyte concentrations in sea and river water, respectively; and M_{water} and ρ_{water} are the water molar mass and density, respectively.

The model made it possible to calculate the generated average power density, $\overline{P_d}$, as shown in Equation (49):

$$\overline{P_d} = \frac{\int_0^L \left(\frac{1}{2} i^2(y) R_{cell}(y)\right) dy}{L}, \tag{49}$$

where L is the length of the RED cell; factor $1/2$ is due to the double membrane area (CEM and AEM) in a cell; and $R_{cell}(y) = R^S(y) + R^R(y) + R^{AEM} + R^{CEM}$ is the area resistance of the RED cell, which depends on the area resistance of the river, R^S, and sea water, R^R, compartments as well as on the resistance of the cation-, R^{CEM}, and anion-exchange, R^{AEM}, membranes. It was assumed that the values of R^{CEM} and R^{AEM} do not depend on y.

The obtained value of $\overline{P_d}$ was close to the experimentally determined value of 1 W/m^2 when using an apparatus equipped with Fumasep FKD cation-exchange membranes and Fumasep FAD anion-exchange membranes (Fumatech, Germany). This result was obtained when the solution residence time in the RED stack chambers was minimal. The main conclusion in relation to the performance of the process was that the IEMs should be as thin as possible and have small resistance.

Within the framework of the classification in Section 4, it can be said that the approach proposed by [15] is close to the "solution-diffusion" approach (TMS model). Similar modeling approaches were used to evaluate the maximum power density of RED systems based on Fumasep membranes FAS-50 and FKS-50 [264,265] and Fujifilm CEM and AEM membranes (Fujifilm, Netherlands) [266]. It is shown that the power density increases significantly with an increase in the concentration of the sea water solution and the Reynolds number.

Tedesco et al. [149] took into account the distribution of concentration not only along the length of each chamber in the RED stack, but also along their width. The membrane was considered as a gel phase (as in the TMS model). Ion transport was described using the Nernst–Planck equation (25) under the LEN assumption (15). Water transport was not taken into account due to the fact that it is small due to the counteracting action of osmosis and electroosmosis. This approach made it possible to take into account the contribution of coion transfer and show that the power density decreases with non-ideality of the membrane. Gurreri et al. presented a similar model [267] but with a membrane that had a profiled surface. They found an elevated flux of coions, which was due to a high concentration of these ions in the membrane caused by their strong concentration in the external solution (seawater).

Moya [268–270] presented a one-dimensional TMS model that takes into account the two-dimensionality of the RED system. In particular, he used the diffusion layer thickness, δ, depending on the longitudinal coordinate y. The Leveque equation [271] was applied:

$$\delta = \frac{h}{1.47}\left(\frac{h^2 v_0}{yD}\right)^{-1/3}, \tag{50}$$

where h is the intermembrane channel width; and v_0 is the average flow rate in the intermembrane channel.

Moya's model makes it possible to investigate the efficiency of the RED process in the presence of doubly charged counterions in electrolyte solutions. It has been shown that the selectivity of membranes decreases as the flux of coions increases due to a decrease in the Donnan exclusion of coions from the IEM. The diffusion coefficient of doubly charged counterions in the membrane is much less than that of singly charged ones, which leads to an additional increase in the resistance of the system. Thus, the efficiency of the RED process decreases in the presence of doubly charged ions in electrolyte solutions.

As a continuation of their work, Tedesco et al. [150] took into account the transport of water through the IEM. To do this, they used the Stefan–Maxwell equation [60]:

$$-\nabla\mu_i = RT\sum_j f_{i-j}(v_i - v_j), \quad (51)$$

where $f_{i\text{-}j}$ is the friction factor between ion I and substance j (which can be the water, the membrane matrix, or another ion); and v_i and v_j are the velocities of i and j.

The fluid flow through the membrane was considered as a function of osmotic and hydrostatic pressure gradients, and the fluid friction against the membrane matrix was taken into account. It was shown that water transport through the membrane causes the decrease in the efficiency of the RED process, and its contribution to this decrease is comparable to the contribution of the coion flux through the membrane. The thickness of the membrane (in the range from 20 to 100 μm) did not significantly affect the maximum power density [272], which was about 1 W/m^2 for the system under study. A similar maximum power density was also obtained by La Cerva et al. [273]. These authors have also shown that membrane profiling allows an increase in gross power density, but reduces net power density due to the loss in the solution pumping.

Davydov et al. [14] were the first to use the microheterogeneous model [157] (see Section 4.1) to estimate the power density of RED. This made it possible to take into account the electrical conductivity and diffusion permeability of the applied membranes over a wide range of concentrations. Despite the fact that the model used was relatively simple and did not take into account the channel geometry or solution flow parameters, the authors have achieved relatively good agreement between the calculated and experimental power density.

Fan et al. [274] applied the Donnan–Manning theory [94] to describe ion sorption in the IEM during the RED process without fitting parameters. Diffusion coefficients were calculated using the Mackie and Meares model [275], taking into account the Manning condensation theory. Two trade-offs are considered in the paper: higher seawater salinity reduces IEM selectivity, but membrane resistance also decreases; and higher water sorption of IEM increases ion diffusivity in its volume, i.e., reduces resistance, but also reduces selectivity due to dilution of fixed charges. Jin et al. [276] also applied the Donnan–Manning and Mackie and Meares theory, which made it possible to eliminate fitting parameters, even in the 2D model, such as ion diffusivity in IEM, resistance and permselectivity coefficients.

There are also other works on modeling the RED process; however, the attention in these studies was mainly on the influence of hydrodynamic conditions [277–283]. In these publications, the membrane was considered as ideally selective [280,281], as an ohmic resistance [277–279,282,284] or its effect was taken into account through the boundary condition [283,285].

Currently, there are no works that present comprehensive models which simultaneously take into account the channel geometry and solution flow parameters as well as the structural and kinetic membrane parameters. Accounting for the Donnan–Manning theory made it possible to describe the counterion condensation effect [274,276], but the membrane in this theory is still homogeneous. The first attempt to evaluate IEM selectivity and power density using a multiphase model [14] was also successful, but only the membrane was considered without reference to the parameters of the RED apparatus. However, the efficiency of the RED process depends on the water and coion fluxes through the membrane, and these fluxes strongly increase in the presence of macropores in the membrane structure. The latter effect can be taken into account when applying a multiphase model.

6. Conclusions

The review shows that although a relatively small number of governing equations are used in modeling ion and water transport in charged membranes, the number of different models is quite large. Models of the two main types differ in their general approach to considering the membrane structure, either as an integral quasi-homogeneous material

("diffusion-solution" models) or as a heterogeneous material consisting of an array of pores and hydrophobic domains containing these pores ("pore-flow" models). Further, in each approach there are numerous variations where certain simplifications and assumptions are applied, and different effects are taken into account. There are rather general models, such as the Teorell–Meyer–Sievers model, and models tailored to describe a particular phenomenon that is important in describing a specific process. An example of models of the second kind are the semi-empirical models of Weber–Newman developed for describing ion and water transport in PEMs used in fuel cells. This model takes into account the specific effect of current-induced water streaming flow on the ion (proton) mobility, while in other applications of IEMS this effect is not significant.

We believe that a consistent presentation of the basics of mathematical modeling of transport phenomena in charged membranes, as well as examples of specific mathematical descriptions will be useful both for beginners and experts in this field of knowledge.

Author Contributions: Writing—original draft preparation, S.M.; computations—A.G.; writing—review and editing—V.N., D.I. and D.A. All authors have read and agreed to the published version of the manuscript.

Funding: The authors acknowledge financial support from the Ministry of Science and Higher Education of the Russian Federation within the State Contract 075-15-2022-1117 from 30 June 2022.

Conflicts of Interest: The authors declare no conflict of interest. The funders had no role in the design of the study; in the collection, analyses, or interpretation of data; in the writing of the manuscript, or in the decision to publish the results.

Nomenclature

Abbreviations

AEM	anion-exchange membrane
BCE	block copolymer electrolyte
BPM	bipolar membranes
CEM	cation-exchange membrane
DBL	diffusion boundary layer
ED	electrodialysis
EDL	electrical double layer
FC	fuel cell
HER	hydrogen evolution reaction
HOR	hydrogen oxidation reaction
IEM	ion-exchange membrane
LE	liquid equilibrated
LEN	local electroneutrality
NF	nanofiltration
NPP	Nernst–Planck–Poisson
OER	oxygen evolution reaction
ORR	oxygen reduction reaction
PEM	proton-exchange membrane
PEMFC	proton exchange membrane fuel cells
PTFE	polytetrafluorethylene
RED	reverse electrodialysis
RFB	redox flow batteries
RO	reverse osmosis
TMS	Teorell–Meyer–Sievers (model)
VE	vapor equilibrated

Symbols

a_i	activity of species i
a_w	water vapor activity
b	distance between two neighboring functional groups
c_i	molar concentration of species i
c_s	molar salt concentration
d	membrane thickness
D	electrolyte diffusion coefficient
D_i	diffusion coefficient of species i
$\vec{E}$	electric field intensity
e	protonic charge
F	Faraday's constant
$\vec{F}$	body force
F_m	morphological factor
f_1	gel phase volume fraction
f_2	intergel electroneutral solution volume fraction
$f_{i\text{-}j}$	friction factor between ion i and substance j
$\vec{g}$	gravitational acceleration
g	activity factor
h	channel width
$\vec{i}$	electric current density
$\vec{i}_F$	Faradaic current density
$\vec{j}_i$	flux density of species i
J_{sub}	substance flux
$\vec{j}_V$	volumetric flux density
k_B	Boltzmann constant
K_D	Donnan equilibrium coefficient
k_p	porous medium hydraulic permeability
K_s	partition coefficient
L	channel length
L_{ij}	phenomenological conductivity coefficient
L_p	hydraulic permeability coefficient
M_{water}	water molar mass
n_{ch}	charged monomer mole fraction
n_{xl}	neutral crosslinker mole fraction
P	diffusion permeability coefficient
p	pressure
p^m	membrane pore volume fraction
$\overline{P_d}$	average power density
P_{sat}	saturation pressure of water
$\overline{Q}$	concentration fixed ions
q	space charge
R	gas constant
R_{cell}	area cell resistance
R_i	generation rate of species i in a chemical reaction
T	temperature
t	time
t_i	transport number of species i
v_0	is the average flow rate
$\vec{v}$	substance movement velocity
V	volume
$\vec{V}$	fluid flow velocity
$\overline{V}_i$	partial molar volume
w	membrane water content
x_{w}	mole fraction of water in the gas
z_i	charge number of species i

z_Q	charge of functional group
Greek Symbols	
α	structural parameter depending on the position of the phases with respect to the transport axis
β	electroosmotic permeability coefficient
γ_i	activity coefficient of species i
δ	diffusion layer thickness
ε	relative permittivity
ε_0	vacuum permittivity
ε_p	polymer dielectric constant
ε_w	water dielectric constant
κ	electrical conductivity
λ_B	Bjerrum length
λ_{eq}	water content (in $H_2O/SO_3{}^-$)
μ	dynamic viscosity
μ_i	electrochemical potential of species i
μ_i^0	standard electrochemical potential of species i
ν	kinematic viscosity
$\nu_\pm$	stoichiometric number
ξ	reduced linear charge density
ξ_{crit}	critical reduced linear charge density
π	osmotic pressure
ρ	density
ρ_e	volumetric charge density
σ	Staverman reflection coefficient
φ	electric potential
ϕ_w	membrane water volume fraction
Δ	difference in a quantity
∇	gradient operator
Indices	
$-$	anion
+	cation
A	coion
c	counterion
g	superscript denoting that the quantity relates to the gel phase
i	species
s	superscript denoting that the quantity relates to the interstitial solution
w	water

References

1. Werber, J.R.; Osuji, C.O.; Elimelech, M. Materials for next-generation desalination and water purification membranes. *Nat. Rev. Mater.* **2016**, *1*, 16018. [CrossRef]
2. Mauter, M.S.; Zucker, I.; Perreault, F.; Werber, J.R.; Kim, J.-H.; Elimelech, M. The role of nanotechnology in tackling global water challenges. *Nat. Sustain.* **2018**, *1*, 166–175. [CrossRef]
3. Al-Amshawee, S.; Yunus, M.Y.B.M.; Azoddein, A.A.M.; Hassell, D.G.; Dakhil, I.H.; Hasan, H.A. Electrodialysis desalination for water and wastewater: A review. *Chem. Eng. J.* **2020**, *380*, 122231. [CrossRef]
4. Gurreri, L.; Tamburini, A.; Cipollina, A.; Micale, G. Electrodialysis Applications in Wastewater Treatment for Environmental Protection and Resources Recovery: A Systematic Review on Progress and Perspectives. *Membranes* **2020**, *10*, 146. [CrossRef]
5. Alkhadra, M.A.; Su, X.; Suss, M.E.; Tian, H.; Guyes, E.N.; Shocron, A.N.; Conforti, K.M.; de Souza, J.P.; Kim, N.; Tedesco, M.; et al. Electrochemical Methods for Water Purification, Ion Separations, and Energy Conversion. *Chem. Rev.* **2022**, *122*, 13547–13635. [CrossRef]
6. Apel, P.Y.; Bobreshova, O.V.; Volkov, A.V.; Volkov, V.V.; Nikonenko, V.V.; Stenina, I.A.; Filippov, A.N.; Yampolskii, Y.P.; Yaroslavtsev, A.B. Prospects of Membrane Science Development. *Membr. Membr. Technol.* **2019**, *1*, 45–63. [CrossRef]
7. Bazinet, L.; Geoffroy, T.R. Electrodialytic Processes: Market Overview, Membrane Phenomena, Recent Developments and Sustainable Strategies. *Membranes* **2020**, *10*, 221. [CrossRef]
8. Du, L.; Prabhakaran, V.; Xie, X.; Park, S.; Wang, Y.; Shao, Y. Low-PGM and PGM-Free Catalysts for Proton Exchange Membrane Fuel Cells: Stability Challenges and Material Solutions. *Adv. Mater.* **2021**, *33*, 1908232. [CrossRef]
9. Luo, T.; Abdu, S.; Wessling, M. Selectivity of ion exchange membranes: A review. *J. Membr. Sci.* **2018**, *555*, 429–454. [CrossRef]

10. Falcão, D.S.; Pinto, A.M.F.R. A review on PEM electrolyzer modelling: Guidelines for beginners. *J. Clean. Prod.* **2020**, *261*, 121184. [CrossRef]
11. Jiang, S.; Sun, H.; Wang, H.; Ladewig, B.P.; Yao, Z. A comprehensive review on the synthesis and applications of ion exchange membranes. *Chemosphere* **2021**, *282*, 130817. [CrossRef] [PubMed]
12. Xiong, P.; Zhang, L.; Chen, Y.; Peng, S.; Yu, G. A Chemistry and Microstructure Perspective on Ion-Conducting Membranes for Redox Flow Batteries. *Angew. Chem. Int. Ed.* **2021**, *60*, 24770–24798. [CrossRef] [PubMed]
13. Logan, B.E.; Elimelech, M. Membrane-based processes for sustainable power generation using water. *Nature* **2012**, *488*, 313–319. [CrossRef]
14. Davydov, D.; Nosova, E.; Loza, S.; Achoh, A.; Korzhov, A.; Sharafan, M.; Melnikov, S. Use of the Microheterogeneous Model to Assess the Applicability of Ion-Exchange Membranes in the Process of Generating Electricity from a Concentration Gradient. *Membranes* **2021**, *11*, 406. [CrossRef] [PubMed]
15. Veerman, J.; Saakes, M.J.; Metz, S.J.; Harmsen, G. Reverse electrodialysis: A validated process model for design and optimization. *Chem. Eng. J.* **2011**, *166*, 256–268. [CrossRef]
16. Tian, H.; Wang, Y.; Pei, Y.; Crittenden, J.C. Unique applications and improvements of reverse electrodialysis: A review and outlook. *Appl. Energy* **2020**, *262*, 114482. [CrossRef]
17. Xu, A.; Shyy, W.; Zhao, T. Lattice Boltzmann modeling of transport phenomena in fuel cells and flow batteries. *Acta Mech. Sin.* **2017**, *33*, 555–574. [CrossRef]
18. Vichard, L.; Steiner, N.Y.; Zerhouni, N.; Hissel, D. Hybrid fuel cell system degradation modeling methods: A comprehensive review. *J. Power Source* **2021**, *506*, 230071. [CrossRef]
19. Ran, J.; Wu, L.; He, Y.; Yang, Z.; Wang, Y.; Jiang, C.; Ge, L.; Bakangura, E.; Xu, T. Ion exchange membranes: New developments and applications. *J. Membr. Sci.* **2017**, *522*, 267–291. [CrossRef]
20. Mizutani, Y. Structure of ion exchange membranes. *J. Membr. Sci.* **1990**, *49*, 121–144. [CrossRef]
21. Sarapulova, V.; Shkorkina, I.; Mareev, S.; Pismenskaya, N.; Kononenko, N.; Larchet, C.; Dammak, L.; Nikonenko, V. Transport Characteristics of Fujifilm Ion-Exchange Membranes as Compared to Homogeneous Membranes AMX and CMX and to Heterogeneous Membranes MK-40 and MA-41. *Membranes* **2019**, *9*, 84. [CrossRef] [PubMed]
22. Nikonenko, V.V.; Mareev, S.A.; Pis'menskaya, N.D.; Uzdenova, A.M.; Kovalenko, A.V.; Urtenov, M.K.; Pourcelly, G. Effect of electroconvection and its use in intensifying the mass transfer in electrodialysis (Review). *Russ. J. Electrochem.* **2017**, *53*, 1122–1144. [CrossRef]
23. Mani, A.; Wang, K.M. Electroconvection Near Electrochemical Interfaces: Experiments, Modeling, and Computation. *Annu. Rev. Fluid Mech.* **2020**, *52*, 509–529. [CrossRef]
24. Kreuer, K.-D.; Paddison, S.J.; Spohr, E.; Schuster, M. Transport in Proton Conductors for Fuel-Cell Applications: Simulations, Elementary Reactions, and Phenomenology. *Chem. Rev.* **2004**, *104*, 4637–4678. [CrossRef]
25. Giorno, L.; Drioli, E.; Strathmann, H. Permselectivity of Ion-Exchange Membranes. In *Encyclopedia of Membranes*; Springer: Berlin/Heidelberg, Germany, 2016; pp. 1490–1493.
26. Zhang, Y.; Paepen, S.; Pinoy, L.; Meesschaert, B.; Van der Bruggen, B. Selectrodialysis: Fractionation of divalent ions from monovalent ions in a novel electrodialysis stack. *Sep. Purif. Technol.* **2012**, *88*, 191–201. [CrossRef]
27. Park, H.B.; Kamcev, J.; Robeson, L.M.; Elimelech, M.; Freeman, B.D. Maximizing the right stuff: The trade-off between membrane permeability and selectivity. *Science* **2017**, *356*, 1138–1148. [CrossRef]
28. Zhang, B.; Gao, H.; Xiao, C.; Tong, X.; Chen, Y. The trade-off between membrane permselectivity and conductivity: A percolation simulation of mass transport. *J. Membr. Sci.* **2020**, *597*, 117751. [CrossRef]
29. Pärnamäe, R.; Mareev, S.; Nikonenko, V.; Melnikov, S.; Sheldeshov, N.; Zabolotskii, V.; Hamelers, H.V.M.; Tedesco, M. Bipolar membranes: A review on principles, latest developments, and applications. *J. Membr. Sci.* **2021**, *617*, 118538. [CrossRef]
30. Weber, A.Z.; Borup, R.L.; Darling, R.M.; Das, P.K.; Dursch, T.J.; Gu, W.; Harvey, D.; Kusoglu, A.; Litster, S.; Mench, M.M.; et al. A Critical Review of Modeling Transport Phenomena in Polymer-Electrolyte Fuel Cells. *J. Electrochem. Soc.* **2014**, *161*, F1254–F1299. [CrossRef]
31. Stenina, I.A.; Yaroslavtsev, A.B. Ionic Mobility in Ion-Exchange Membranes. *Membranes* **2021**, *11*, 198. [CrossRef]
32. Douglin, J.C.; Varcoe, J.R.; Dekel, D.R. A high-temperature anion-exchange membrane fuel cell. *J. Power Sources Adv.* **2020**, *5*, 100023. [CrossRef]
33. Van Rijn, P.; Tutus, M.; Kathrein, C.; Zhu, L.; Wessling, M.; Schwaneberg, U.; Böker, A. Challenges and advances in the field of self-assembled membranes. *Chem. Soc. Rev.* **2013**, *42*, 6578–6592. [CrossRef] [PubMed]
34. Timashev, S.F. *Physical Chemistry of Membrane Processes*; Ellis Horwood Ltd.: New York, NY, USA, 1991; ISBN 9780136629825.
35. Mauritz, K.A.; Moore, R.B. State of Understanding of Nafion. *Chem. Rev.* **2004**, *104*, 4535–4586. [CrossRef] [PubMed]
36. Gebel, G. Structural evolution of water swollen perfluorosulfonated ionomers from dry membrane to solution. *Polymer* **2000**, *41*, 5829–5838. [CrossRef]
37. Helfferich, F.G. *Ion Exchange*; McGraw-Hill/Dover Publications: New York, NY, USA, 1995; Volume 138, ISBN 0486687848.
38. Drozdov, A.D.; de Claville Christiansen, J. The effects of pH and ionic strength on equilibrium swelling of polyampholyte gels. *Int. J. Solids Struct.* **2017**, *110–111*, 192–208. [CrossRef]

39. Kozmai, A.E.; Nikonenko, V.V.; Zyryanova, S.; Pismenskaya, N.D.; Dammak, L.; Baklouti, L. Modelling of anion-exchange membrane transport properties with taking into account the change in exchange capacity and swelling when varying bathing solution concentration and pH. *J. Membr. Sci.* **2019**, *590*, 117291. [CrossRef]
40. Gierke, T.D.; Munn, G.E.; Wilson, F.C. The morphology in nafion perfluorinated membrane products, as determined by wide- and small-angle X-ray studies. *J. Polym. Sci. Polym. Phys. Ed.* **1981**, *19*, 1687–1704. [CrossRef]
41. Kreuer, K.D. On the development of proton conducting polymer membranes for hydrogen and methanol fuel cells. *J. Membr. Sci.* **2001**, *185*, 29–39. [CrossRef]
42. Berezina, N.P.; Kononenko, N.A.; Dyomina, O.A.; Gnusin, N.P. Characterization of ion-exchange membrane materials: Properties vs structure. *Adv. Colloid Interface Sci.* **2008**, *139*, 3–28. [CrossRef]
43. Kononenko, N.; Nikonenko, V.; Grande, D.; Larchet, C.; Dammak, L.; Fomenko, M.; Volfkovich, Y. Porous structure of ion exchange membranes investigated by various techniques. *Adv. Colloid Interface Sci.* **2017**, *246*, 196–216. [CrossRef]
44. Svoboda, M.; Beneš, J.; Vobecká, L.; Slouka, Z. Swelling induced structural changes of a heterogeneous cation-exchange membrane analyzed by micro-computed tomography. *J. Membr. Sci.* **2017**, *525*, 195–201. [CrossRef]
45. Zvaigzne, M.A.; Martynov, I.L.; Samokhvalov, P.S.; Nabiev, I.R. Fabrication of composite materials from semiconductor quantum dots and organic polymers for optoelectronics and biomedicine: Role of surface ligands. *Russ. Chem. Bull.* **2016**, *65*, 2568–2577. [CrossRef]
46. Donnan, F.G. The theory of membrane equilibrium and membrane potential in the presence of a non-dialyzable electrolyte. A contribution to physical-chemical physiology. *Z. Elektrochem. Angew. Phys. Chem.* **1911**, *17*, 572–581.
47. Shiryaeva, I.M.; Victorov, A.I. Equilibrium of ion-exchange polymeric membrane with aqueous salt solution and its thermodynamic modeling. *Fluid Phase Equilibria* **2001**, *180*, 115–138. [CrossRef]
48. Paddison, S.J.; Bender, G.; Kreuer, K.D.; Nicoloso, N.; Zawodzinski, T.A. The microwave region of the dielectric spectrum of hydrated Nafion®and other sulfonated membranes. *J. New Mater. Electrochem. Syst.* **2000**, *3*, 291–300.
49. Paddison, S.J.; Reagor, D.W.; Zawodzinski, T.A., Jr. High frequency dielectric studies of hydrated Nafion®. *J. Electroanal. Chem.* **1998**, *459*, 91–97. [CrossRef]
50. Haubold, H.-G.; Vad, T.; Jungbluth, H.; Hiller, P. Nano structure of NAFION: A SAXS study. *Electrochim. Acta* **2001**, *46*, 1559–1563. [CrossRef]
51. Kornyshev, A.A.; Kuznetsov, A.M.; Spohr, E.; Ulstrup, J. Kinetics of Proton Transport in Water. *J. Phys. Chem. B* **2003**, *107*, 3351–3366. [CrossRef]
52. Nikonenko, V.V.; Yaroslavtsev, A.B.; Pourcelly, G. Ion Transfer in and Through Charged Membranes: Structure, Properties, and Theory. In *Ionic Interactions in Natural and Synthetic Macromolecules*; John Wiley & Sons Inc.: Hoboken, NJ, USA, 2012; pp. 267–335. ISBN 9780470529270.
53. Lu, Z. State of water in perfluorosulfonic acid membranes. *J. Electrochem. Soc.* **2005**, *155*, 67–68.
54. Paddison, S.J. Proton Conduction Mechanisms at Low Degrees of Hydration in Sulfonic Acid–Based Polymer Electrolyte Membranes. *Annu. Rev. Mater. Res.* **2003**, *33*, 289–319. [CrossRef]
55. Zhou, X.; Wang, Z.; Epsztein, R.; Zhan, C.; Li, W.; Fortner, J.D.; Pham, T.A.; Kim, J.-H.; Elimelech, M. Intrapore energy barriers govern ion transport and selectivity of desalination membranes. *Sci. Adv.* **2020**, *6*, eabd9045. [CrossRef] [PubMed]
56. Larchet, C.; Nouri, S.; Auclair, B.; Dammak, L.; Nikonenko, V. Application of chronopotentiometry to determine the thickness of diffusion layer adjacent to an ion-exchange membrane under natural convection. *Adv. Colloid Interface Sci.* **2008**, *139*, 45–61. [CrossRef] [PubMed]
57. Goh, P.S.; Ismail, A.F. A review on inorganic membranes for desalination and wastewater treatment. *Desalination* **2018**, *434*, 60–80. [CrossRef]
58. Dickinson, E.J.F.; Smith, G. Modelling the Proton-Conductive Membrane in Practical Polymer Electrolyte Membrane Fuel Cell (PEMFC) Simulation: A Review. *Membranes* **2020**, *10*, 310. [CrossRef] [PubMed]
59. Tanaka, Y. Ion Exchange Membranes. In *Fundamentals and Applications*, 2nd ed.; Elsevier Science: Amsterdam, The Netherlands, 2015; ISBN 9780444633194.
60. Newman, J.S.; Balsara, N.P. *Electrochemical Systems*, 4th ed.; Wiley-Blackwell: Hoboken, NJ, USA, 2021; ISBN 9781119514602.
61. Nikonenko, V.; Nebavsky, A.; Mareev, S.; Kovalenko, A.; Urtenov, M.; Pourcelly, G.; Nikonenko, V.; Nebavsky, A.; Mareev, S.; Kovalenko, A.; et al. Modelling of Ion Transport in Electromembrane Systems: Impacts of Membrane Bulk and Surface Heterogeneity. *Appl. Sci.* **2018**, *9*, 25. [CrossRef]
62. Soetaert, K.; Herman, P.M.J. *A practical Guide to Ecological Modelling: Using R as a Simulation Platform*; Soetaert, K., Herman, P.M.J., Eds.; Springer: Dordrecht, The Netherlands, 2009; ISBN 9781402086236.
63. Bear, J. *Dynamics of Fluids in Porous Media (Dover Civil and Mechanical Engineering)*; Dover Publications: New York, NY, USA, 1988; ISBN 9780486656755.
64. Liu, J.-L. Poisson's Equation in Electrostatics. Available online: https://dasher.wustl.edu/chem430/readings/poisson-equation.pdf (accessed on 16 December 2022).
65. Cohen, H.; Cooley, J.W. The Numerical Solution of the Time-Dependent Nernst-Planck Equations. *Biophys. J.* **1965**, *5*, 145–162. [CrossRef]
66. Uzdenova, A.; Kovalenko, A.; Urtenov, M.; Nikonenko, V. 1D Mathematical Modelling of Non-Stationary Ion Transfer in the Diffusion Layer Adjacent to an Ion-Exchange Membrane in Galvanostatic Mode. *Membranes* **2018**, *8*, 84. [CrossRef]

67. Moya, A.A. Electrochemical Impedance of Ion-Exchange Membranes in Ternary Solutions with Two Counterions. *J. Phys. Chem. C* **2014**, *118*, 2539–2553. [CrossRef]
68. Yaroshchuk, A.; Zhu, Y.; Bondarenko, M.; Bruening, M.L. Deviations from Electroneutrality in Membrane Barrier Layers: A Possible Mechanism Underlying High Salt Rejections. *Langmuir* **2016**, *32*, 2644–2658. [CrossRef]
69. Kilic, M.S.; Bazant, M.Z.; Ajdari, A. Steric effects in the dynamics of electrolytes at large applied voltages. II. Modified Poisson-Nernst-Planck equations. *Phys. Rev. E* **2007**, *75*, 021503. [CrossRef]
70. Golubenko, D.V.; Yaroslavtsev, A.B. Effect of current density, concentration of ternary electrolyte and type of cations on the monovalent ion selectivity of surface-sulfonated graft anion-exchange membranes: Modelling and experiment. *J. Membr. Sci.* **2021**, *635*, 119466. [CrossRef]
71. Gorobchenko, A.; Mareev, S.; Nikonenko, V. Mathematical Modeling of Monovalent Permselectivity of a Bilayer Ion-Exchange Membrane as a Function of Current Density. *Int. J. Mol. Sci.* **2022**, *23*, 4711. [CrossRef] [PubMed]
72. Honarparvar, S.; Reible, D. Modeling multicomponent ion transport to investigate selective ion removal in electrodialysis. *Environ. Sci. Ecotechnol.* **2020**, *1*, 100007. [CrossRef]
73. Mareev, S.A.; Evdochenko, E.; Wessling, M.; Kozaderova, O.A.; Niftaliev, S.I.; Pismenskaya, N.D.; Nikonenko, V.V. A comprehensive mathematical model of water splitting in bipolar membranes: Impact of the spatial distribution of fixed charges and catalyst at bipolar junction. *J. Membr. Sci.* **2020**, *603*, 118010. [CrossRef]
74. Skolotneva, E.; Tsygurina, K.; Mareev, S.; Melnikova, E.; Pismenskaya, N.; Nikonenko, V. High Diffusion Permeability of Anion-Exchange Membranes for Ammonium Chloride: Experiment and Modeling. *Int. J. Mol. Sci.* **2022**, *23*, 5782. [CrossRef]
75. Yaroshchuk, A.; Bruening, M.L.; Zholkovskiy, E. Modelling nanofiltration of electrolyte solutions. *Adv. Colloid Interface Sci.* **2019**, *268*, 39–63. [CrossRef]
76. Kedem, O.; Katchalsky, A. Permeability of composite membranes. Part 1.—Electric current, volume flow and flow of solute through membranes. *Trans. Faraday Soc.* **1963**, *59*, 1918–1930. [CrossRef]
77. Meares, P. Coupling of ion and water fluxes in synthetic membranes. *J. Membr. Sci.* **1981**, *8*, 295–307. [CrossRef]
78. Koter, S.; Kujawski, W.; Koter, I. Importance of the cross-effects in the transport through ion-exchange membranes. *J. Membr. Sci.* **2007**, *297*, 226–235. [CrossRef]
79. Auclair, B.; Nikonenko, V.; Larchet, C.; Métayer, M.; Dammak, L. Correlation between transport parameters of ion-exchange membranes. *J. Membr. Sci.* **2002**, *195*, 89–102. [CrossRef]
80. Sarapulova, V.; Pismenskaya, N.; Butylskii, D.; Titorova, V.; Wang, Y.; Xu, T.; Zhang, Y.; Nikonenko, V. Transport and Electrochemical Characteristics of CJMCED Homogeneous Cation Exchange Membranes in Sodium Chloride, Calcium Chloride, and Sodium Sulfate Solutions. *Membranes* **2020**, *10*, 165. [CrossRef] [PubMed]
81. Rubinstein, I.; Schur, A.; Zaltzman, B. Artifact of "Breakthrough" osmosis: Comment on the local Spiegler-Kedem-Katchalsky equations with constant coefficients. *Sci. Rep.* **2021**, *11*, 5051. [CrossRef]
82. Jarzyńska, M.; Staryga, E.; Kluza, F.; Spiess, W.E.L.; Góral, D. Diffusion Characteristics in Ethyl Alcohol and Glucose Solutions Using Kedem-Katchalsky Equations. *Chem. Eng. Technol.* **2020**, *43*, 248–252. [CrossRef]
83. Kujawski, W.; Yaroshchuk, A.; Zholkovskiy, E.; Koter, I.; Koter, S. Analysis of Membrane Transport Equations for Reverse Electrodialysis (RED) Using Irreversible Thermodynamics. *Int. J. Mol. Sci.* **2020**, *21*, 6325. [CrossRef] [PubMed]
84. Hidalgo, A.M.; León, G.; Gómez, M.; Murcia, M.D.; Gómez, E.; Macario, J.A. Removal of different dye solutions: A comparison study using a polyamide nf membrane. *Membranes* **2020**, *10*, 408. [CrossRef] [PubMed]
85. De Jaegher, B.; De Schepper, W.; Verliefde, A.; Nopens, I. A model-based analysis of electrodialysis fouling during pulsed electric field operation. *J. Membr. Sci.* **2022**, *642*, 119975. [CrossRef]
86. Rybalkina, O.A.; Sharafan, M.V.; Nikonenko, V.V.; Pismenskaya, N.D. Two mechanisms of H+/OH− ion generation in anion-exchange membrane systems with polybasic acid salt solutions. *J. Membr. Sci.* **2022**, *651*, 120449. [CrossRef]
87. Kimani, E.M.; Pranić, M.; Porada, S.; Kemperman, A.J.B.; Ryzhkov, I.I.; van der Meer, W.G.J.; Biesheuvel, P.M. The influence of feedwater pH on membrane charge ionization and ion rejection by reverse osmosis: An experimental and theoretical study. *J. Membr. Sci.* **2022**, *660*, 120800. [CrossRef]
88. Zhang, L.; Biesheuvel, P.M.; Ryzhkov, I.I. Theory of Ion and Water Transport in Electron-Conducting Membrane Pores with p H-Dependent Chemical Charge. *Phys. Rev. Appl.* **2019**, *12*, 014039. [CrossRef]
89. Chen, G. Donnan equilibrium revisited: Coupling between ion concentrations, osmotic pressure, and donnan potential. *J. Micromech. Mol. Phys.* **2022**, *07*, 127–134. [CrossRef]
90. Robinson, R.A.; Stokes, R.H. *Electrolyte Solutions*, 2nd ed.; Butterworths: London, UK, 2002; ISBN 0-486-42225-9.
91. Miller, D.G. Application of Irreversible Thermodynamics to Electrolyte Solutions. I. Determination of Ionic Transport Coefficients l ij for Isothermal Vector Transport Processes in Binary Electrolyte Systems 1,2. *J. Phys. Chem.* **1966**, *70*, 2639–2659. [CrossRef]
92. Münchinger, A.; Kreuer, K.-D. Selective ion transport through hydrated cation and anion exchange membranes I. The effect of specific interactions. *J. Membr. Sci.* **2019**, *592*, 117372. [CrossRef]
93. Tran, T.; Lin, C.; Chaurasia, S.; Lin, H. Elucidating the relationship between states of water and ion transport properties in hydrated polymers. *J. Membr. Sci.* **2019**, *574*, 299–308. [CrossRef]
94. Kamcev, J.; Galizia, M.; Benedetti, F.M.; Jang, E.-S.; Paul, D.R.; Freeman, B.D.; Manning, G.S. Partitioning of mobile ions between ion exchange polymers and aqueous salt solutions: Importance of counter-ion condensation. *Phys. Chem. Chem. Phys.* **2016**, *18*, 6021–6031. [CrossRef] [PubMed]

95. Manning, G.S. Limiting Laws and Counterion Condensation in Polyelectrolyte Solutions I. Colligative Properties. *J. Chem. Phys.* **1969**, *51*, 924–933. [CrossRef]
96. Manning, G.S. Polyelectrolytes. *Annu. Rev. Phys. Chem.* **1972**, *23*, 117–140. [CrossRef]
97. Bockris, J.O.; Reddy, A.K.N. *Modern Electrochemistry*, 2nd ed.; Springer: Berlin/Heidelberg, Germany, 1998; ISBN 0306455552.
98. Kitto, D.; Kamcev, J. Manning condensation in ion exchange membranes: A review on ion partitioning and diffusion models. *J. Polym. Sci.* **2022**, *60*, 2929–2973. [CrossRef]
99. Kamcev, J.; Paul, D.R.; Freeman, B.D. Ion Activity Coefficients in Ion Exchange Polymers: Applicability of Manning's Counterion Condensation Theory. *Macromolecules* **2015**, *48*, 8011–8024. [CrossRef]
100. Jang, E.-S.; Kamcev, J.; Kobayashi, K.; Yan, N.; Sujanani, R.; Talley, S.J.; Moore, R.B.; Paul, D.R.; Freeman, B.D. Effect of Water Content on Sodium Chloride Sorption in Cross-Linked Cation Exchange Membranes. *Macromolecules* **2019**, *52*, 2569–2579. [CrossRef]
101. Yu, Y.; Yan, N.; Freeman, B.D.; Chen, C. Mobile ion partitioning in ion exchange membranes immersed in saline solutions. *J. Membr. Sci.* **2021**, *620*, 118760. [CrossRef]
102. Yan, N.; Paul, D.R.; Freeman, B.D. Water and ion sorption in a series of cross-linked AMPS/PEGDA hydrogel membranes. *Polymer* **2018**, *146*, 196–208. [CrossRef]
103. Ji, Y.; Luo, H.; Geise, G.M. Specific co-ion sorption and diffusion properties influence membrane permselectivity. *J. Membr. Sci.* **2018**, *563*, 492–504. [CrossRef]
104. Chang, K.; Luo, H.; Geise, G.M. Water content, relative permittivity, and ion sorption properties of polymers for membrane desalination. *J. Membr. Sci.* **2019**, *574*, 24–32. [CrossRef]
105. Chang, K.; Luo, H.; Bannon, S.M.; Lin, S.Y.; Agata, W.-A.S.; Geise, G.M. Methoxy groups increase water and decrease salt permeability properties of sulfonated polysulfone desalination membranes. *J. Membr. Sci.* **2021**, *630*, 119298. [CrossRef]
106. Galizia, M.; Paul, D.R.; Freeman, B.D. Co-ion specific effect on sodium halides sorption and transport in a cross-linked poly(p-styrene sulfonate-co-divinylbenzene) for membrane applications. *J. Membr. Sci.* **2020**, *612*, 118410. [CrossRef]
107. Galizia, M.; Manning, G.S.; Paul, D.R.; Freeman, B.D. Ion partitioning between brines and ion exchange polymers. *Polymer* **2019**, *165*, 91–100. [CrossRef]
108. Chen, G.Q.; Wei, K.; Hassanvand, A.; Freeman, B.D.; Kentish, S.E. Single and binary ion sorption equilibria of monovalent and divalent ions in commercial ion exchange membranes. *Water Res.* **2020**, *175*, 115681. [CrossRef]
109. Kingsbury, R.S.; Zhu, S.; Flotron, S.; Coronell, O. Microstructure Determines Water and Salt Permeation in Commercial Ion-Exchange Membranes. *ACS Appl. Mater. Interfaces* **2018**, *10*, 39745–39756. [CrossRef]
110. Wang, Q.; Chen, G.Q.; Kentish, S.E. Sorption and diffusion of organic acid ions in anion exchange membranes: Acetate and lactate ions as a case study. *J. Membr. Sci.* **2020**, *614*, 118534. [CrossRef]
111. Kusoglu, A.; Weber, A.Z. New Insights into Perfluorinated Sulfonic-Acid Ionomers. *Chem. Rev.* **2017**, *117*, 987–1104. [CrossRef]
112. Sujanani, R.; Katz, L.E.; Paul, D.R.; Freeman, B.D. Aqueous ion partitioning in Nafion: Applicability of Manning's counter-ion condensation theory. *J. Membr. Sci.* **2021**, *638*, 119687. [CrossRef]
113. Ramos-Garcés, M.V.; Li, K.; Lei, Q.; Bhattacharya, D.; Kole, S.; Zhang, Q.; Strzalka, J.; Angelopoulou, P.P.; Sakellariou, G.; Kumar, R.; et al. Understanding the ionic activity and conductivity value differences between random copolymer electrolytes and block copolymer electrolytes of the same chemistry. *RSC Adv.* **2021**, *11*, 15078–15084. [CrossRef] [PubMed]
114. Lei, Q.; Li, K.; Bhattacharya, D.; Xiao, J.; Kole, S.; Zhang, Q.; Strzalka, J.; Lawrence, J.; Kumar, R.; Arges, C.G. Counterion condensation or lack of solvation? Understanding the activity of ions in thin film block copolymer electrolytes. *J. Mater. Chem. A* **2020**, *8*, 15962–15975. [CrossRef]
115. Ritt, C.L.; Werber, J.R.; Wang, M.; Yang, Z.; Zhao, Y.; Kulik, H.J.; Elimelech, M. Ionization behavior of nanoporous polyamide membranes. *Proc. Natl. Acad. Sci. USA* **2020**, *117*, 30191–30200. [CrossRef]
116. Wang, J.; Kingsbury, R.S.; Perry, L.A.; Coronell, O. Partitioning of Alkali Metal Salts and Boric Acid from Aqueous Phase into the Polyamide Active Layers of Reverse Osmosis Membranes. *Environ. Sci. Technol.* **2017**, *51*, 2295–2303. [CrossRef]
117. Chang, K.; Luo, H.; Geise, G.M. Influence of Salt Concentration on Hydrated Polymer Relative Permittivity and State of Water Properties. *Macromolecules* **2021**, *54*, 637–646. [CrossRef]
118. Chang, K.; Geise, G.M. Dielectric Permittivity Properties of Hydrated Polymers: Measurement and Connection to Ion Transport Properties. *Ind. Eng. Chem. Res.* **2020**, *59*, 5205–5217. [CrossRef]
119. Baker, R.W. *Membrane Technology and Applications*, 3rd ed.; John Wiley and Sons Ltd.: New York, NY, USA, 2012; ISBN 9780470743720.
120. Yaroshchuk, A.E.; Dukhin, S.S. Phenomenological theory of reverse osmosis in macroscopically homogeneous membranes and its specification for the capillary space-charge model. *J. Membr. Sci.* **1993**, *79*, 133–158. [CrossRef]
121. Choy, T.C. *Effective Medium Theory: Principles and Applications*; Oxford University Press: Oxford, UK, 2015; ISBN 0198518927.
122. Teorell, T. An Attempt to Formulate a Quantitative Theory of Membrane Permeability. *Proc. Soc. Exp. Biol. Med.* **1935**, *33*, 282–285. [CrossRef]
123. Meyer, K.H.; Sievers, J.F. La perméabilité des membranes I. Théorie de la perméabilité ionique. *Helv. Chim. Acta* **1936**, *19*, 649–664. [CrossRef]
124. Tanaka, Y. Chapter 4 Theory of Teorell, Meyer and Sievers (TMS Theory). *Membr. Sci. Technol.* **2007**, *12*, 59–66. [CrossRef]

125. Nikonenko, V.; Lebedev, K.; Manzanares, J.A.; Pourcelly, G. Modelling the transport of carbonic acid anions through anion-exchange membranes. *Electrochim. Acta* **2003**, *48*, 3639–3650. [CrossRef]
126. Murphy, W.D.; Manzanares, J.A.; Mafe, S.; Reiss, H. A numerical study of the equilibrium and nonequilibrium diffuse double layer in electrochemical cells. *J. Phys. Chem.* **1992**, *96*, 9983–9991. [CrossRef]
127. Rossi, M.; Wallmersperger, T. Thermodynamically consistent three-dimensional electrochemical model for polymeric membranes. *Electrochim. Acta* **2018**, *283*, 1323–1338. [CrossRef]
128. Titorova, V.D.; Mareev, S.A.; Gorobchenko, A.D.; Gil, V.V.; Nikonenko, V.V.; Sabbatovskii, K.G.; Pismenskaya, N.D. Effect of current-induced coion transfer on the shape of chronopotentiograms of cation-exchange membranes. *J. Membr. Sci.* **2021**, *624*, 119036. [CrossRef]
129. Wang, X.-L.; Tsuru, T.; Nakao, S.-i.; Kimura, S. Electrolyte transport through nanofiltration membranes by the space-charge model and the comparison with Teorell-Meyer-Sievers model. *J. Membr. Sci.* **1995**, *103*, 117–133. [CrossRef]
130. Galama, A.H.; Post, J.W.; Hamelers, H.V.M.; Nikonenko, V.V.; Biesheuvel, P.M. On the Origin of the Membrane Potential Arising Across Densely Charged Ion Exchange Membranes: How Well Does the Teorell-Meyer-Sievers Theory Work? *J. Membr. Sci. Res.* **2016**, *2*, 128–140. [CrossRef]
131. Yan, Z.; Zhu, L.; Li, Y.C.; Wycisk, R.J.; Pintauro, P.N.; Hickner, M.A.; Mallouk, T.E. The balance of electric field and interfacial catalysis in promoting water dissociation in bipolar membranes. *Energy Environ. Sci.* **2018**, *11*, 2235–2245. [CrossRef]
132. Vermaas, D.A.; Wiegman, S.; Nagaki, T.; Smith, W.A. Ion transport mechanisms in bipolar membranes for (photo)electrochemical water splitting. *Sustain. Energy Fuels* **2018**, *2*, 2006–2015. [CrossRef]
133. Strathmann, H.; Krol, J.; Rapp, H.-J.; Eigenberger, G. Limiting current density and water dissociation in bipolar membranes. *J. Membr. Sci.* **1997**, *125*, 123–142. [CrossRef]
134. Wrubel, J.A.; Chen, Y.; Ma, Z.; Deutsch, T.G. Modeling Water Electrolysis in Bipolar Membranes. *J. Electrochem. Soc.* **2020**, *167*, 114502. [CrossRef]
135. Culcasi, A.; Gurreri, L.; Zaffora, A.; Cosenza, A.; Tamburini, A.; Micale, G. On the modelling of an Acid/Base Flow Battery: An innovative electrical energy storage device based on pH and salinity gradients. *Appl. Energy* **2020**, *277*, 115576. [CrossRef]
136. Ortega, A.; Arenas, L.F.; Pijpers, J.J.H.; Vicencio, D.L.; Martínez, J.C.; Rodríguez, F.A.; Rivero, E.P. Modelling water dissociation, acid-base neutralization and ion transport in bipolar membranes for acid-base flow batteries. *J. Membr. Sci.* **2022**, *641*, 119899. [CrossRef]
137. Yan, Z.; Wycisk, R.J.; Metlay, A.S.; Xiao, L.; Yoon, Y.; Pintauro, P.N.; Mallouk, T.E. High-Voltage Aqueous Redox Flow Batteries Enabled by Catalyzed Water Dissociation and Acid–Base Neutralization in Bipolar Membranes. *ACS Cent. Sci.* **2021**, *7*, 1028–1035. [CrossRef] [PubMed]
138. Dykstra, J.E.; Heijne, A.; Puig, S.; Biesheuvel, P. Theory of transport and recovery in microbial electrosynthesis of acetate from CO_2. *Electrochim. Acta* **2021**, *379*, 138029. [CrossRef]
139. Bui, J.C.; Corpus, K.R.M.; Bell, A.T.; Weber, A.Z. On the Nature of Field-Enhanced Water Dissociation in Bipolar Membranes. *J. Phys. Chem. C* **2021**, *125*, 24974–24987. [CrossRef]
140. Lin, M.; Digdaya, I.A.; Xiang, C. Modeling the electrochemical behavior and interfacial junction profiles of bipolar membranes at solar flux relevant operating current densities. *Sustain. Energy Fuels* **2021**, *5*, 2149–2158. [CrossRef]
141. Hurwitz, H.D.; Dibiani, R. Experimental and theoretical investigations of steady and transient states in systems of ion exchange bipolar membranes. *J. Membr. Sci.* **2004**, *228*, 17–43. [CrossRef]
142. León, T.; López, J.; Torres, R.; Grau, J.; Jofre, L.; Cortina, J.-L. Describing ion transport and water splitting in an electrodialysis stack with bipolar membranes by a 2-D model: Experimental validation. *J. Membr. Sci.* **2022**, *660*, 120835. [CrossRef]
143. Achoh, A.R.; Zabolotsky, V.I.; Lebedev, K.A.; Sharafan, M.V.; Yaroslavtsev, A.B. Electrochemical Properties and Selectivity of Bilayer Ion-Exchange Membranes in Ternary Solutions of Strong Electrolytes. *Membr. Membr. Technol.* **2021**, *3*, 52–71. [CrossRef]
144. Zabolotsky, V.I.; Achoh, A.R.; Lebedev, K.A.; Melnikov, S.S. Permselectivity of bilayered ion-exchange membranes in ternary electrolyte. *J. Membr. Sci.* **2020**, *608*, 118152. [CrossRef]
145. Melnikova, E.D.; Pismenskaya, N.D.; Bazinet, L.; Mikhaylin, S.; Nikonenko, V.V. Effect of ampholyte nature on current-voltage characteristic of anion-exchange membrane. *Electrochim. Acta* **2018**, *285*, 185–191. [CrossRef]
146. Sarapulova, V.; Nevakshenova, E.; Pismenskaya, N.; Dammak, L.; Nikonenko, V. Unusual concentration dependence of ion-exchange membrane conductivity in ampholyte-containing solutions: Effect of ampholyte nature. *J. Membr. Sci.* **2015**, *479*, 28–38. [CrossRef]
147. Titorova, V.D.; Moroz, I.A.; Mareev, S.A.; Pismenskaya, N.D.; Sabbatovskii, K.G.; Wang, Y.; Xu, T.; Nikonenko, V.V. How bulk and surface properties of sulfonated cation-exchange membranes response to their exposure to electric current during electrodialysis of a Ca2+ containing solution. *J. Membr. Sci.* **2022**, *644*, 120149. [CrossRef]
148. Zhang, W.; Yan, H.; Wang, Q.; Zhao, C. An extended Teorell-Meyer-Sievers theory for membrane potential under non-isothermal conditions. *J. Membr. Sci.* **2022**, *643*, 120073. [CrossRef]
149. Tedesco, M.; Hamelers, H.V.M.; Biesheuvel, P.M.M. Nernst-Planck transport theory for (reverse) electrodialysis: I. Effect of co-ion transport through the membranes. *J. Membr. Sci.* **2016**, *510*, 370–381. [CrossRef]
150. Tedesco, M.; Hamelers, H.V.M.; Biesheuvel, P.M. Nernst-Planck transport theory for (reverse) electrodialysis: II. Effect of water transport through ion-exchange membranes. *J. Membr. Sci.* **2017**, *531*, 172–182. [CrossRef]

151. Gurreri, L.; Filingeri, A.; Ciofalo, M.; Cipollina, A.; Tedesco, M.; Tamburini, A.; Micale, G. Electrodialysis with asymmetrically profiled membranes: Influence of profiles geometry on desalination performance and limiting current phenomena. *Desalination* **2021**, *506*, 115001. [CrossRef]
152. Forrest, T.; Höfler, L.; Bakker, E. Dialysis membranes as liquid junction materials: Simplified model based on the phase boundary potential. *J. Electroanal. Chem.* **2022**, *904*, 115886. [CrossRef]
153. Fíla, V.; Bouzek, K. *The Effect of Convection in the External Diffusion Layer on the Results of a Mathematical Model of Multiple Ion Transport across an Ion-Selective Membrane*; Springer: Dordrecht, The Netherlands, 2008; Volume 38, pp. 1241–1252.
154. Fíla, V.; Bouzek, K. A Mathematical Model of Multiple Ion Transport across an Ion-Selective Membrane under Current Load Conditions. *J. Appl. Electrochem.* **2003**, *33*, 675–684. [CrossRef]
155. Sokirko, A.V.; Manzanares, J.A.; Pellicer, J. The Permselectivity of Membrane Systems with an Inhomogeneous Distribution of Fixed Charge Groups. *J. Colloid Interface Sci.* **1994**, *168*, 32–39. [CrossRef]
156. Moya, A.A.; Moleón, J.A. Study of the electrical properties of bi-layer ion-exchange membrane systems. *J. Electroanal. Chem.* **2010**, *647*, 53–59. [CrossRef]
157. Zabolotsky, V.I.; Nikonenko, V.V. Effect of structural membrane inhomogeneity on transport properties. *J. Membr. Sci.* **1993**, *79*, 181–198. [CrossRef]
158. Berezina, N.P.; Gnusin, N.P.; Demina, O.A.; Annikova, L.A. Effect of polyaniline on the current passing through structural fragments of ion-exchange sulfonic-cationite resins and membranes. *Russ. J. Electrochem.* **2009**, *45*, 1226–1233. [CrossRef]
159. Mafé, S.; Manzanares, J.A.; Pellicer, J. On the introduction of the pore wall charge in the space-charge model for microporous membranes. *J. Membr. Sci.* **1990**, *51*, 161–168. [CrossRef]
160. Hsu, W.Y.; Gierke, T.D. Ion transport and clustering in nafion perfluorinated membranes. *J. Membr. Sci.* **1983**, *13*, 307–326. [CrossRef]
161. Filippov, A.N. A Cell Model of an Ion-Exchange Membrane. Capillary-Osmosis and Reverse-Osmosis Coefficients. *Colloid J.* **2022**, *84*, 332–343. [CrossRef]
162. Dubinin, M.M. Surface and Porosity of Adsorbents. *Russ. Chem. Rev.* **1982**, *51*, 605–611. [CrossRef]
163. Gnusin, N.P.; Zabolotsky, V.I.; Nikonenko, V.V.; Meshechkov, A.I. Development of the generalized conductance principle to the description of transfer phenomena in disperse systems under the acting of different forces. *Russ. J. Phys. Chem.* **1980**, *54*, 1518–1522.
164. Gnusin, N.P.; Berezina, N.P.; Kononenko, N.A.; Dyomina, O.A. Transport structural parameters to characterize ion exchange membranes. *J. Membr. Sci.* **2004**, *243*, 301–310. [CrossRef]
165. Porozhnyy, M.; Huguet, P.; Cretin, M.; Safronova, E.; Nikonenko, V. Mathematical modeling of transport properties of proton-exchange membranes containing immobilized nanoparticles. *Int. J. Hydrogen Energy* **2016**, *41*, 15605–15614. [CrossRef]
166. Nichka, V.S.; Mareev, S.A.; Porozhnyy, M.V.; Shkirskaya, S.A.; Safronova, E.Y.; Pismenskaya, N.D.; Nikonenko, V.V. Modified Microheterogeneous Model for Describing Electrical Conductivity of Membranes in Dilute Electrolyte Solutions. *Membr. Membr. Technol.* **2019**, *1*, 190–199. [CrossRef]
167. Kozmai, A.; Pismenskaya, N.; Nikonenko, V. Mathematical Description of the Increase in Selectivity of an Anion-Exchange Membrane Due to Its Modification with a Perfluorosulfonated Ionomer. *Int. J. Mol. Sci.* **2022**, *23*, 2238. [CrossRef] [PubMed]
168. Melnikov, S.; Kolot, D.; Nosova, E.; Zabolotskiy, V. Peculiarities of transport-structural parameters of ion-exchange membranes in solutions containing anions of carboxylic acids. *J. Membr. Sci.* **2018**, *557*, 1–12. [CrossRef]
169. Manohar, M.; Thakur, A.K.; Pandey, R.P.; Shahi, V.K. Efficient and stable anion exchange membrane: Tuned membrane permeability and charge density for molecular/ionic separation. *J. Membr. Sci.* **2015**, *496*, 250–258. [CrossRef]
170. Niftaliev, S.I.; Kozaderova, O.A.; Kim, K.B. Electroconductance of heterogeneous ion-exchange membranes in aqueous salt solutions. *J. Electroanal. Chem.* **2017**, *794*, 58–63. [CrossRef]
171. Sedkaoui, Y.; Szymczyk, A.; Lounici, H.; Arous, O. A new lateral method for characterizing the electrical conductivity of ion-exchange membranes. *J. Membr. Sci.* **2016**, *507*, 34–42. [CrossRef]
172. Tong, X.; Zhang, B.; Fan, Y.; Chen, Y. Mechanism Exploration of Ion Transport in Nanocomposite Cation Exchange Membranes. *ACS Appl. Mater. Interfaces* **2017**, *9*, 13491–13499. [CrossRef]
173. Kudashova, D.S.; Kononenko, N.A.; Brovkina, M.A.; Falina, I.V. A Study of the Degradation of a Perfluorinated Membrane during Operation in a Proton-Exchange Membrane Fuel Cell. *Membr. Membr. Technol.* **2022**, *4*, 23–30. [CrossRef]
174. Falina, I.; Loza, N.; Loza, S.; Titskaya, E.; Romanyuk, N. Permselectivity of Cation Exchange Membranes Modified by Polyaniline. *Membranes* **2021**, *11*, 227. [CrossRef]
175. Salmeron-Sanchez, I.; Asenjo-Pascual, J.; Avilés-Moreno, J.R.; Ocón, P. Microstructural description of ion exchange membranes: The effect of PPy-based modification. *J. Membr. Sci.* **2022**, *659*, 120771. [CrossRef]
176. Pismenskaya, N.D.; Nevakshenova, E.E.; Nikonenko, V.V. Using a Single Set of Structural and Kinetic Parameters of the Microheterogeneous Model to Describe the Sorption and Kinetic Properties of Ion-Exchange Membranes. *Pet. Chem.* **2018**, *58*, 465–473. [CrossRef]
177. Falina, I.V.; Kononenko, N.A.; Demina, O.A.; Titskaya, E.V.; Loza, S.A. Estimation of Ion-Exchange Equilibrium Constant Using Membrane Conductivity Data. *Colloid J.* **2021**, *83*, 379–386. [CrossRef]

178. Golubenko, D.V.; Karavanova, Y.A.; Melnikov, S.S.; Achoh, A.R.; Pourcelly, G.; Yaroslavtsev, A.B. An approach to increase the permselectivity and mono-valent ion selectivity of cation-exchange membranes by introduction of amorphous zirconium phosphate nanoparticles. *J. Membr. Sci.* **2018**, *563*, 777–784. [CrossRef]
179. Le, X.T. Permselectivity and microstructure of anion exchange membranes. *J. Colloid Interface Sci.* **2008**, *325*, 215–222. [CrossRef] [PubMed]
180. Kozmai, A.; Nikonenko, V.; Pismenskaya, N.; Dammak, L.; Baklouti, L.; Yutskevich, Y. Effect of anion exchange membrane capacity loss on pH and electric conductivity of saline solution during neutralization dialysis. *J. Membr. Sci.* **2020**, *595*, 117573. [CrossRef]
181. Sarapulova, V.V.; Titorova, V.D.; Nikonenko, V.V.; Pismenskaya, N.D. Transport Characteristics of Homogeneous and Heterogeneous Ion-Exchange Membranes in Sodium Chloride, Calcium Chloride, and Sodium Sulfate Solutions. *Membr. Membr. Technol.* **2019**, *1*, 168–182. [CrossRef]
182. Perreault, V.; Sarapulova, V.; Tsygurina, K.; Pismenskaya, N.; Bazinet, L. Understanding of Adsorption and Desorption Mechanisms of Anthocyanins and Proanthocyanidins on Heterogeneous and Homogeneous Cation-Exchange Membranes. *Membranes* **2021**, *11*, 136. [CrossRef]
183. Tuan, L.X.; Buess-Herman, C. Study of water content and microheterogeneity of CMS cation exchange membrane. *Chem. Phys. Lett.* **2007**, *434*, 49–55. [CrossRef]
184. Zabolotsky, V.I.; Lebedev, K.A.; Nikonenko, V.V.; Shudrenko, A.A. Identification of a microheterogeneous model for a heterogeneous membrane. *Russ. J. Electrochem.* **1993**, *29*, 811–816.
185. Wyllie, M.R.J.; Southwick, P.F. An Experimental Investigation of the S.P. and Resistivity Phenomena in Dirty Sands. *J. Pet. Technol.* **1954**, *6*, 44–57. [CrossRef]
186. Sauer, M.C.; Southwick, P.F.; Spiegler, K.S.; Wyllie, M.R.J. Electrical Conductance of Porous Plugs—Ion Exchange Resin-Solution Systems. *Ind. Eng. Chem.* **1955**, *47*, 2187–2193. [CrossRef]
187. Spiegler, K.S.; Yoest, R.L.; Wyllie, M.R.J. Electrical potentials across porous plugs and membranes. Ion-exchange resin-solution systems. *Discuss. Faraday Soc.* **1956**, *21*, 174–185. [CrossRef]
188. Narębska, A.; Wódzki, R. Diffusion of electrolytes across inhomogeneous permselective membranes. *Die Angew. Makromol. Chem.* **1979**, *80*, 105–118. [CrossRef]
189. Wódzki, R.; Narebska, A. Composition and structure of cation permselective membranes II. Multilayer electrochemical model. *Angew. Makromol. Chem.* **1980**, *88*, 149–163. [CrossRef]
190. Demina, O.A.; Kononenko, N.A.; Falina, I.V. New approach to the characterization of ion-exchange membranes using a set of model parameters. *Pet. Chem.* **2014**, *54*, 515–525. [CrossRef]
191. Filippov, A.N.; Safronova, E.Y.; Yaroslavtsev, A.B. Theoretical and experimental investigation of diffusion permeability of hybrid MF-4SC membranes with silica nanoparticles. *J. Membr. Sci.* **2014**, *471*, 110–117. [CrossRef]
192. Filippov, A.; Khanukaeva, D.; Afonin, D.; Skorikova, G.; Ivanov, E.; Vinokurov, V.; Lvov, Y. Transport Properties of Novel Hybrid Cation-Exchange Membranes on the Base of MF-4SC and Halloysite Nanotubes. *J. Mater. Sci. Chem. Eng.* **2015**, *03*, 58–65. [CrossRef]
193. Filippov, A.; Afonin, D.; Kononenko, N.; Lvov, Y.; Vinokurov, V. New approach to characterization of hybrid nanocomposites. *Colloids Surf. A Physicochem. Eng. Asp.* **2017**, *521*, 251–259. [CrossRef]
194. Happel, J.; Brenner, H. *Low Reynolds Number Hydrodynamics*; Springer: Berlin/Heidelberg, Germany, 1973; ISBN 9789024728770.
195. Deo, S.; Filippov, A.; Tiwari, A.; Vasin, S.; Starov, V. Hydrodynamic permeability of aggregates of porous particles with an impermeable core. *Adv. Colloid Interface Sci.* **2011**, *164*, 21–37. [CrossRef]
196. Filippov, A.N. A Cell Model of an Ion-Exchange Membrane. Hydrodynamic Permeability. *Colloid J.* **2018**, *80*, 716–727. [CrossRef]
197. Vasin, S.I.; Filippov, A.N.; Starov, V.M. Hydrodynamic permeability of membranes built up by particles covered by porous shells: Cell models. *Adv. Colloid Interface Sci.* **2008**, *139*, 83–96. [CrossRef] [PubMed]
198. Filippov, A.N. A Cell Model of the Ion-Exchange Membrane. Electrical Conductivity and Electroosmotic Permeability. *Colloid J.* **2018**, *80*, 728–738. [CrossRef]
199. Brinkman, H.C. A calculation of the viscous force exerted by a flowing fluid on a dense swarm of particles. *Flow Turbul. Combust.* **1949**, *1*, 27. [CrossRef]
200. Filippov, A.N.; Shkirskaya, S.A. Approbation of the Cell Model of a Cation-Exchange Membrane on 1:1 Electrolytes. *Membr. Membr. Technol.* **2019**, *1*, 278–285. [CrossRef]
201. Filippov, A.N.; Kononenko, N.A.; Loza, N.V.; Kopitsyn, D.S.; Petrova, D.A. Modelling of transport properties of perfluorinated one- and bilayer membranes modified by polyaniline decorated clay nanotubes. *Electrochim. Acta* **2021**, *389*, 138768. [CrossRef]
202. Yadav, P.K.; Tiwari, A.; Singh, P. Hydrodynamic permeability of a membrane built up by spheroidal particles covered by porous layer. *Acta Mech.* **2018**, *229*, 1869–1892. [CrossRef]
203. Yadav, P.K.; Deo, S.; Singh, S.P.; Filippov, A. Effect of magnetic field on the hydrodynamic permeability of a membrane built up by porous spherical particles. *Colloid J.* **2017**, *79*, 160–171. [CrossRef]
204. Tang, C.; Yaroshchuk, A.; Bruening, M.L. Flow through negatively charged, nanoporous membranes separates Li+ and K+ due to induced electromigration. *Chem. Commun.* **2020**, *56*, 10954–10957. [CrossRef]
205. Kislyi, A.G.; Butylskii, D.Y.; Mareev, S.A.; Nikonenko, V.V. Model of Competitive Ion Transfer in an Electro-Baromembrane System with Track-Etched Membrane. *Membr. Membr. Technol.* **2021**, *3*, 131–138. [CrossRef]

206. Wijmans, J.G.; Baker, R.W. The solution-diffusion model: A review. *J. Membr. Sci.* **1995**, *107*, 1–21. [CrossRef]
207. García-Morales, V.; Cervera, J.; Manzanares, J.A. Pore entrance effects on the electrical potential distribution in charged porous membranes and ion channels. *J. Electroanal. Chem.* **2007**, *599*, 203–208. [CrossRef]
208. Sparreboom, W.; van den Berg, A.; Eijkel, J.C.T. Principles and applications of nanofluidic transport. *Nat. Nanotechnol.* **2009**, *4*, 713–720. [CrossRef] [PubMed]
209. Bazant, M.Z.; Squires, T.M. Induced-charge electrokinetic phenomena. *Curr. Opin. Colloid Interface Sci.* **2010**, *15*, 203–213. [CrossRef]
210. Yaroshchuk, A.; Boiko, Y.; Makovetskiy, A. Ion-Rejection, Electrokinetic and Electrochemical Properties of a Nanoporous Track-Etched Membrane and Their Interpretation by Means of Space Charge Model. *Langmuir* **2009**, *25*, 9605–9614. [CrossRef] [PubMed]
211. Szymczyk, A.; Zhu, H.; Balannec, B. Ion Rejection Properties of Nanopores with Bipolar Fixed Charge Distributions. *J. Phys. Chem. B* **2010**, *114*, 10143–10150. [CrossRef] [PubMed]
212. Peters, P.B.; van Roij, R.; Bazant, M.Z.; Biesheuvel, P.M. Analysis of electrolyte transport through charged nanopores. *Phys. Rev. E* **2016**, *93*, 053108. [CrossRef]
213. Moya, A.A.; Nikonenko, V.V. A comparative theoretical study of potential distribution and conductivity in cation- and anion-exchange nanoporous membranes filled with ternary electrolytes. *Electrochim. Acta* **2015**, *180*, 929–938. [CrossRef]
214. Ryzhkov, I.I.; Lebedev, D.V.; Solodovnichenko, V.S.; Shiverskiy, A.V.; Simunin, M.M. Induced-Charge Enhancement of the Diffusion Potential in Membranes with Polarizable Nanopores. *Phys. Rev. Lett.* **2017**, *119*, 226001. [CrossRef]
215. Catalano, J.; Hamelers, H.V.M.; Bentien, A.; Biesheuvel, P.M. Revisiting Morrison and Osterle 1965: The efficiency of membrane-based electrokinetic energy conversion. *J. Phys. Condens. Matter* **2016**, *28*, 324001. [CrossRef]
216. Szymczyk, A.; Zhu, H.; Balannec, B. Pressure-Driven Ionic Transport through Nanochannels with Inhomogenous Charge Distributions. *Langmuir* **2010**, *26*, 1214–1220. [CrossRef] [PubMed]
217. Balannec, B.; Ghoufi, A.; Szymczyk, A. Nanofiltration performance of conical and hourglass nanopores. *J. Membr. Sci.* **2018**, *552*, 336–340. [CrossRef]
218. Chen, Y.-T.; Hsu, J.-P. Pressure-driven power generation and ion separation using a non-uniformly charged nanopore. *J. Colloid Interface Sci.* **2022**, *607*, 1120–1130. [CrossRef] [PubMed]
219. Liu, Z.; Liu, X.; Wang, Y.; Yang, D.; Li, C. Ion current rectification in asymmetric charged bilayer nanochannels. *Electrochim. Acta* **2022**, *403*, 139706. [CrossRef]
220. Wu, C.-T.; Hsu, J.-P. Electrokinetic behavior of bullet-shaped nanopores modified by functional groups: Influence of finite thickness of modified layer. *J. Colloid Interface Sci.* **2021**, *582*, 741–751. [CrossRef]
221. Han, W.; Chen, X. A review: Applications of ion transport in micro-nanofluidic systems based on ion concentration polarization. *J. Chem. Technol. Biotechnol.* **2020**, *95*, 1622–1631. [CrossRef]
222. Hsu, J.-P.; Su, T.-C.; Lin, C.-Y.; Tseng, S. Power generation from a pH-regulated nanochannel through reverse electrodialysis: Effects of nanochannel shape and non-uniform H+ distribution. *Electrochim. Acta* **2019**, *294*, 84–92. [CrossRef]
223. Ryzhkov, I.I.; Lebedev, D.V.; Solodovnichenko, V.S.; Minakov, A.V.; Simunin, M.M. On the origin of membrane potential in membranes with polarizable nanopores. *J. Membr. Sci.* **2018**, *549*, 616–630. [CrossRef]
224. Ryzhkov, I.I.; Minakov, A.V. Theoretical study of electrolyte transport in nanofiltration membranes with constant surface potential/charge density. *J. Membr. Sci.* **2016**, *520*, 515–628. [CrossRef]
225. Ryzhkov, I.I.; Shchurkina, M.A.; Mikhlina, E.V.; Simunin, M.M.; Nemtsev, I.V. Switchable ionic selectivity of membranes with electrically conductive surface: Theory and experiment. *Electrochim. Acta* **2021**, *375*, 137970. [CrossRef]
226. Ryzhkov, I.I.; Vyatkin, A.S.; Mikhlina, E.V. Modelling of Conductive Nanoporous Membranes with Switchable Ionic Selectivity. *Membr. Membr. Technol.* **2020**, *2*, 10–19. [CrossRef]
227. Bocquet, L.; Charlaix, E. Nanofluidics, from bulk to interfaces. *Chem. Soc. Rev.* **2010**, *39*, 1073–1095. [CrossRef] [PubMed]
228. Guzmán-Garcia, A.G.; Pintauro, P.N.; Verbrugge, M.W.; Hill, R.F. Development of a space-charge transport model for ion-exchange membranes. *AIChE J.* **1990**, *36*, 1061–1074. [CrossRef]
229. Eikerling, M.; Kornyshev, A.A. Proton transfer in a single pore of a polymer electrolyte membrane. *J. Electroanal. Chem.* **2001**, *502*, 1–14. [CrossRef]
230. Biesheuvel, P.M.; Bazant, M.Z. Analysis of ionic conductance of carbon nanotubes. *Phys. Rev. E* **2016**, *94*, 050601. [CrossRef]
231. Zangle, T.A.; Mani, A.; Santiago, J.G. Theory and experiments of concentration polarization and ion focusing at microchannel and nanochannel interfaces. *Chem. Soc. Rev.* **2010**, *39*, 1014–1035. [CrossRef]
232. Melnikov, D.V.; Hulings, Z.K.; Gracheva, M.E. Electro-osmotic flow through nanopores in thin and ultrathin membranes. *Phys. Rev. E* **2017**, *95*, 063105. [CrossRef]
233. Mansouri, A.; Scheuerman, C.; Bhattacharjee, S.; Kwok, D.Y.; Kostiuk, L.W. Transient streaming potential in a finite length microchannel. *J. Colloid Interface Sci.* **2005**, *292*, 567–580. [CrossRef]
234. Yang, Y.; Pintauro, P.N. Multicomponent space-charge transport model for ion-exchange membranes. *AIChE J.* **2000**, *46*, 1177–1190. [CrossRef]
235. Höltzel, A.; Tallarek, U. Ionic conductance of nanopores in microscale analysis systems: Where microfluidics meets nanofluidics. *J. Sep. Sci.* **2007**, *30*, 1398–1419. [CrossRef]
236. Schoch, R.B.; Han, J.; Renaud, P. Transport phenomena in nanofluidics. *Rev. Mod. Phys.* **2008**, *80*, 839–883. [CrossRef]

237. Bazant, M.Z.; Kilic, M.S.; Storey, B.D.; Ajdari, A. Towards an understanding of induced-charge electrokinetics at large applied voltages in concentrated solutions. *Adv. Colloid Interface Sci.* **2009**, *152*, 48–88. [CrossRef] [PubMed]
238. Cwirko, E.H.; Carbonell, R.G. Interpretation of transport coefficients in Nafion using a parallel pore model. *J. Membr. Sci.* **1992**, *67*, 227–247. [CrossRef]
239. Szymczyk, A.; Fievet, P.; Aoubiza, B.; Simon, C.; Pagetti, J. An application of the space charge model to the electrolyte conductivity inside a charged microporous membrane. *J. Membr. Sci.* **1999**, *161*, 275–285. [CrossRef]
240. Narębska, A.; Koter, S.; Kujawski, W. Ions and water transport across charged nafion membranes. Irreversible thermodynamics approach. *Desalination* **1984**, *51*, 3–17. [CrossRef]
241. Zhu, Z.; Wang, D.; Tian, Y.; Jiang, L. Ion/Molecule Transportation in Nanopores and Nanochannels: From Critical Principles to Diverse Functions. *J. Am. Chem. Soc.* **2019**, *141*, 8658–8669. [CrossRef]
242. Kurupath, V.P.; Kannam, S.K.; Hartkamp, R.; Sathian, S.P. Highly efficient water desalination through hourglass shaped carbon nanopores. *Desalination* **2021**, *505*, 114978. [CrossRef]
243. Chen, Y.; Liu, Y.; Xu, Y.; Guo, X.; Cao, Y.; Ming, W. Review: Modeling and Simulation of Membrane Electrode Material Structure for Proton Exchange Membrane Fuel Cells. *Coatings* **2022**, *12*, 1145. [CrossRef]
244. Zhao, J.; Li, X.; Shum, C.; McPhee, J. A Review of physics-based and data-driven models for real-time control of polymer electrolyte membrane fuel cells. *Energy AI* **2021**, *6*, 100114. [CrossRef]
245. Zhang, G.; Jiao, K. Multi-phase models for water and thermal management of proton exchange membrane fuel cell: A review. *J. Power Source* **2018**, *391*, 120–133. [CrossRef]
246. Olivier, P.; Bourasseau, C.; Bouamama, P.B. Low-temperature electrolysis system modelling: A review. *Renew. Sustain. Energy Rev.* **2017**, *78*, 280–300. [CrossRef]
247. Jahnke, T.; Futter, G.; Latz, A.; Malkow, T.; Papakonstantinou, G.; Tsotridis, G.; Schott, P.; Gérard, M.; Quinaud, M.; Quiroga, M.; et al. Performance and degradation of Proton Exchange Membrane Fuel Cells: State of the art in modeling from atomistic to system scale. *J. Power Sources* **2016**, *304*, 207–233. [CrossRef]
248. Chen, Q.; Wang, Y.; Yang, F.; Xu, H. Two-dimensional multi-physics modeling of porous transport layer in polymer electrolyte membrane electrolyzer for water splitting. *Int. J. Hydrogen Energy* **2020**, *45*, 32984–32994. [CrossRef]
249. Manso, A.P.; Marzo, F.F.; Barranco, J.; Garikano, X.; Garmendia Mujika, M. Influence of geometric parameters of the flow fields on the performance of a PEM fuel cell. A review. *Int. J. Hydrogen Energy* **2012**, *37*, 15256–15287. [CrossRef]
250. Yang, Z.; Du, Q.; Jia, Z.; Yang, C.; Jiao, K. Effects of operating conditions on water and heat management by a transient multi-dimensional PEMFC system model. *Energy* **2019**, *183*, 462–476. [CrossRef]
251. Zhang, G.; Xie, X.; Xie, B.; Du, Q.; Jiao, K. Large-scale multi-phase simulation of proton exchange membrane fuel cell. *Int. J. Heat Mass Transf.* **2018**, *130*, 555–563. [CrossRef]
252. Zhang, H.; Rahman, M.A.; Mojica, F.; Sui, P.; Chuang, P.A. A comprehensive two-phase proton exchange membrane fuel cell model coupled with anisotropic properties and mechanical deformation of the gas diffusion layer. *Electrochim. Acta* **2021**, *382*, 138273. [CrossRef]
253. Zhao, J.; Li, X. Oxygen transport in polymer electrolyte membrane fuel cells based on measured electrode pore structure and mass transport properties. *Energy Convers. Manag.* **2019**, *186*, 570–585. [CrossRef]
254. Yin, C.; Gao, Y.; Li, T.; Xie, G.; Li, K.; Tang, H. Study of internal multi-parameter distributions of proton exchange membrane fuel cell with segmented cell device and coupled three-dimensional model. *Renew. Energy* **2020**, *147*, 650–662. [CrossRef]
255. Yin, Y.; Wang, X.; Shangguan, X.; Zhang, J.; Qin, Y. Numerical investigation on the characteristics of mass transport and performance of PEMFC with baffle plates installed in the flow channel. *Int. J. Hydrogen Energy* **2018**, *43*, 8048–8062. [CrossRef]
256. Tsukamoto, T.; Aoki, T.; Kanesaka, H.; Taniguchi, T.; Takayama, T.; Motegi, H.; Takayama, R.; Tanaka, S.; Komiyama, K.; Yoneda, M. Three-dimensional numerical simulation of full-scale proton exchange membrane fuel cells at high current densities. *J. Power Source* **2021**, *488*, 229412. [CrossRef]
257. Schiffer, L.; Shirsath, A.V.; Raël, S.; Bonnet, C.; Lapicque, F.; Bessler, W.G. Electrochemical Pressure Impedance Spectroscopy for Polymer Electrolyte Membrane Fuel Cells: A Combined Modeling and Experimental Analysis. *J. Electrochem. Soc.* **2022**, *169*, 034503. [CrossRef]
258. Bagherighajari, F.; Ramiar, A.; Abdollahzadehsangroudi, M.; Páscoa, J.C.; Oliveira, P.J. Numerical simulation of the polymer electrolyte membrane fuel cells with intermediate blocked interdigitated flow fields. *Int. J. Energy Res.* **2022**, *46*, 15309–15331. [CrossRef]
259. Springer, T.E.; Zawodzinski, T.A.; Gottesfeld, S. Polymer Electrolyte Fuel Cell Model. *J. Electrochem. Soc.* **1991**, *138*, 2334–2342. [CrossRef]
260. Weber, A.Z.; Newman, J. Transport in Polymer-Electrolyte Membranes. *J. Electrochem. Soc.* **2004**, *151*, A311–A325. [CrossRef]
261. Zawodzinski, T.A.; Neeman, M.; Sillerud, L.O.; Gottesfeld, S. Determination of water diffusion coefficients in perfluorosulfonate ionomeric membranes. *J. Phys. Chem.* **1991**, *95*, 6040–6044. [CrossRef]
262. Barnoon, P.; Toghraie, D.; Mehmandoust, B.; Fazilati, M.A.; Eftekhari, S.A. Numerical modeling of species transport and functional characteristics of a proton exchange membrane fuel cell using an agglomerate model with a multi-phase model. *Energy Rep.* **2022**, *8*, 11343–11362. [CrossRef]

263. Tian, P.; Liu, X.; Luo, K.; Li, H.; Wang, Y. Deep learning from three-dimensional multiphysics simulation in operational optimization and control of polymer electrolyte membrane fuel cell for maximum power. *Appl. Energy* **2021**, *288*, 116632. [CrossRef]
264. Ortiz-Imedio, R.; Gomez-Coma, L.; Fallanza, M.; Ortiz, A.; Ibañez, R.; Ortiz, I. Comparative performance of Salinity Gradient Power-Reverse Electrodialysis under different operating conditions. *Desalination* **2019**, *457*, 8–21. [CrossRef]
265. Tristán, C.; Pérez, G.; Fallanza, M.; Ortiz, A.; Ibañez, R.; Ortiz, I. A comprehensive study on the effects of operation variables on reverse electrodialysis performance. *Desalination* **2020**, *482*, 114389. [CrossRef]
266. Tedesco, M.; Cipollina, A.; Tamburini, A.; van Baak, W.; Micale, G. Modelling the Reverse ElectroDialysis process with seawater and concentrated brines. *Desalin. Water Treat.* **2012**, *49*, 404–424. [CrossRef]
267. Gurreri, L.; Battaglia, G.; Tamburini, A.; Cipollina, A.; Micale, G.; Ciofalo, M. Multi-physical modelling of reverse electrodialysis. *Desalination* **2017**, *423*, 52–64. [CrossRef]
268. Moya, A.A. Numerical simulation of ionic transport processes through bilayer ion-exchange membranes in reverse electrodialysis stacks. *J. Membr. Sci.* **2017**, *524*, 400–408. [CrossRef]
269. Moya, A.A. A Nernst-Planck analysis on the contributions of the ionic transport in permeable ion-exchange membranes to the open circuit voltage and the membrane resistance in reverse electrodialysis stacks. *Electrochim. Acta* **2017**, *238*, 134–141. [CrossRef]
270. Moya, A.A. Uphill transport in improved reverse electrodialysis by removal of divalent cations in the dilute solution: A Nernst-Planck based study. *J. Membr. Sci.* **2020**, *598*, 117784. [CrossRef]
271. Leveque, M.A. Transmission de chaleur par convection. *Les Lois Transm.* **1928**, *13*, 204.
272. Tedesco, M.; Hamelers, H.V.M.; Biesheuvel, P.M. Nernst-Planck transport theory for (reverse) electrodialysis: III. Optimal membrane thickness for enhanced process performance. *J. Membr. Sci.* **2018**, *565*, 480–487. [CrossRef]
273. La Cerva, M.L.; Di Liberto, M.; Gurreri, L.; Tamburini, A.; Cipollina, A.; Micale, G.; Ciofalo, M. Coupling CFD with a one-dimensional model to predict the performance of reverse electrodialysis stacks. *J. Membr. Sci.* **2017**, *541*, 595–610. [CrossRef]
274. Fan, H.; Yin, N. Elucidating conductivity-permselectivity tradeoffs in electrodialysis and reverse electrodialysis by structure-property analysis of ion-exchange membranes. *J. Membr. Sci.* **2019**, *573*, 668–681. [CrossRef]
275. Mackie, J.S.; Meares, P. The diffusion of electrolytes in a cation-exchange resin membrane I. Theoretical. *Proc. R. Soc. London. Ser. A Math. Phys. Sci.* **1955**, *232*, 498–509. [CrossRef]
276. Jin, D.; Xi, R.; Xu, S.; Wang, P.; Wu, X. Numerical simulation of salinity gradient power generation using reverse electrodialysis. *Desalination* **2021**, *512*, 115132. [CrossRef]
277. Tedesco, M.; Mazzola, P.; Tamburini, A.; Micale, G.; Bogle, I.D.L.; Papapetrou, M.; Cipollina, A. Analysis and simulation of scale-up potentials in reverse electrodialysis. *Desalin. Water Treat.* **2015**, *55*, 3391–3403. [CrossRef]
278. Chen, M.; Mei, Y.; Yu, Y.; Zeng, R.J.; Zhang, F.; Zhou, S.; Tang, C.Y. An internal-integrated RED/ED system for energy-saving seawater desalination: A model study. *Energy* **2019**, *170*, 139–148. [CrossRef]
279. Saleem, M.W.; Jande, Y.A.C.; Kim, W.S. Performance optimization of integrated electrochemical capacitive deionization and reverse electrodialysis model through a series pass desorption process. *J. Electroanal. Chem.* **2017**, *795*, 41–50. [CrossRef]
280. Kim, M.; Kim, S.; Choi, J.; Kim, H.; Jeong, N.; Kwak, R. Numerical analysis of real-scale reverse electrodialysis with microscale structures and electrode segmentation. *Chem. Eng. J.* **2022**, *446*, 137357. [CrossRef]
281. Pawlowski, S.; Geraldes, V.; Crespo, J.G.; Velizarov, S. Computational fluid dynamics (CFD) assisted analysis of profiled membranes performance in reverse electrodialysis. *J. Membr. Sci.* **2016**, *502*, 179–190. [CrossRef]
282. Dong, F.; Jin, D.; Xu, S.; Xu, L.; Wu, X.; Wang, P.; Leng, Q.; Xi, R. Numerical simulation of flow and mass transfer in profiled membrane channels for reverse electrodialysis. *Chem. Eng. Res. Des.* **2020**, *157*, 77–91. [CrossRef]
283. Jalili, Z.; Pharoah, J.; Stokke Burheim, O.; Einarsrud, K. Temperature and Velocity Effects on Mass and Momentum Transport in Spacer-Filled Channels for Reverse Electrodialysis: A Numerical Study. *Energies* **2018**, *11*, 2028. [CrossRef]
284. Moya, A.A. A numerical comparison of optimal load and internal resistances in ion-exchange membrane systems under reverse electrodialysis conditions. *Desalination* **2016**, *392*, 25–33. [CrossRef]
285. He, Z.; Gao, X.; Zhang, Y.; Wang, Y.; Wang, J. Revised spacer design to improve hydrodynamics and anti-fouling behavior in reverse electrodialysis processes. *Desalin. Water Treat.* **2016**, *57*, 28176–28186. [CrossRef]

Disclaimer/Publisher's Note: The statements, opinions and data contained in all publications are solely those of the individual author(s) and contributor(s) and not of MDPI and/or the editor(s). MDPI and/or the editor(s) disclaim responsibility for any injury to people or property resulting from any ideas, methods, instructions or products referred to in the content.